Materials Science in Semiconductor Processing 179 (2024) 108518

Contents lists available at ScienceDirect

Materials Science in Semiconductor Processing

journal homepage: www.elsevier.com/locate/mssp

Review

Immobilization of TiO_2 and ZnO by facile surface engineering methods to improve semiconductor performance in photocatalytic wastewater treatment: A review

Amir Hossein Navidpour [a], Bentuo Xu [b], Mohammad Boshir Ahmed [c], John L. Zhou [a,*]

[a] Centre for Green Technology, School of Civil and Environmental Engineering, University of Technology Sydney, 15 Broadway, Ultimo, NSW, 2007, Australia
[b] School of Life and Environmental Science, Wenzhou University, Wenzhou, 325035, China
[c] Institute for Sustainability, Energy and Resources, School of Chemical Engineering, The University of Adelaide, North Terrace, SA 5005, Australia

ARTICLE INFO

Keywords:
Immobilization
Photocatalysis
Surface engineering
TiO_2
ZnO

ABSTRACT

Photocatalysis is widely researched in water and wastewater treatment processes owing to its unique capacity in the potential mineralization of organic pollutants. Suspended nanoparticles provide high specific surface area, but their practical application has been very limited due to drawbacks such as catalyst agglomeration during treatment and difficulty of catalyst reuse after treatment. It is therefore of paramount importance to immobilize catalysts to realize continuous photocatalysis operations towards commercial scale, and surface engineering provides an ideal strategy to overcome the problems associated with using suspended nanoparticles. Of different semiconductors used for the photocatalytic degradation of organic pollutants, TiO_2 is considered a benchmark photocatalyst with ZnO as a potential alternative. Hence, the scope of this research is to review the application of several surface engineering methods including physical vapor deposition, dip coating, spin coating, spray coating, and electrophoretic deposition in the immobilization of TiO_2 and ZnO. Overall, electrophoretic deposition is considered very promising for the successful immobilization of photocatalysts, and sintering particularly is recommended to improve the adhesion strength of the as-deposited films, expediting the practical applications of photocatalysis through electrophoretic deposition.

1. Introduction

Because of the extensive information base and scientific knowledge, wastewater treatment has begun to focus on the health issues regarding toxic chemicals introduced into the environment [1]. Among the various methods used for the removal of organic pollutants from water, advanced oxidation processes (AOPs) have received attention since the strong oxidants are capable of degrading recalcitrant organic pollutants [2]. Notably, AOPs lead to the oxidation with mineralization of organic pollutants using the production of reactive oxygen species (ROS) including sulfate, hydroxyl, and superoxide radicals [3], where hydroxyl radicals and sulfate radicals are the most powerful oxidizing radicals used to remove the organic pollutants from water [4]. There are several AOPs that can provide complete decomposition of different types of pollutants [5]. AOPs are divided into ozone-based treatment, ultraviolet-based treatment, advanced electrochemical oxidation methods, photo-advanced oxidation methods, and catalytic advanced oxidation methods [4]. Photocatalysis is considered a specific type of chemical transformations and takes the advantage of the energy provided by light [6]. Photocatalysis technology has been widely used for the degradation of various organic pollutants, in addition, it has been applied in other fields, e.g. disinfection, H_2 production, CO_2 reduction, and air purification [7].

Different semiconductors such as tin oxide [8], iron oxide [9], zinc ferrite [10,11], zinc stannate [12,13], graphitic carbon nitride [14,15], titanium dioxide [16,17], and zinc oxide [18,19] have been used for photocatalysis. Noteworthy, development in the synthesis of TiO_2 nanoparticles has initiated its application in various fields like water splitting, CO_2 reduction, food, water purification, air pollution mitigation, and surface disinfection, due to the features of TiO_2 including self-cleaning properties, eco-friendliness, and inert and stable nature [20]. In addition, TiO_2 has been used for H_2 production, anti-fogging surfaces, anticorrosion applications, photovoltaic cells, and photochromism [21]. Generally, TiO_2 can take advantages of its low cost,

* Corresponding author.
E-mail address: junliang.zhou@uts.edu.au (J.L. Zhou).

https://doi.org/10.1016/j.mssp.2024.108518
Received 14 March 2024; Received in revised form 21 April 2024; Accepted 7 May 2024
Available online 15 May 2024

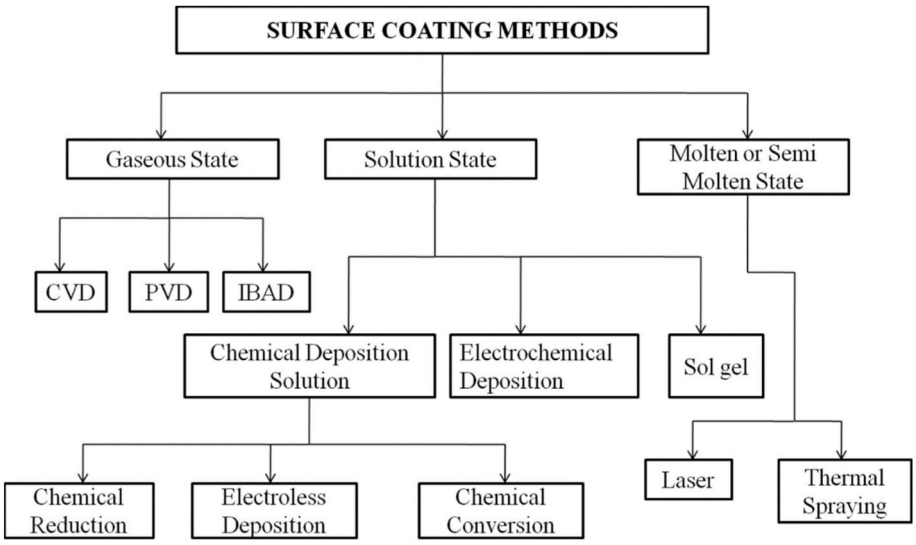

Fig. 1. Classification of surface coating methods. Reproduced with permission from Ref. [40] Copyright 2021 Springer Nature. The rights of this figure are owned by a third party.

outstanding electronic and optical properties, environmental friendliness, high photocatalytic performance, non-toxicity, and high chemical stability [22]; and is considered the most common material used for photocatalytic applications [21]. Hence, various methods have been used to produce titania nanoparticles with numerous morphologies such as nanorods, dendrites, nanodots, hollow spheres, nanobelts, anodic grids, nanoflowers, and 2D nanosheets [20]. Notably, TiO_2 has three main crystal structures including rutile, anatase, and brookite with different stabilities [23].

With its advantages including high chemical stability, facile preparation, great oxidation capacity, low toxicity, and tunable size, n-type ZnO is promising for the photocatalytic decomposition of organic pollutants [24]. Noteworthy, ZnO is considered a potential alternative to TiO_2, where its band gap energy is close to that of TiO_2 [18], however, its photo-absorption ability is greater than TiO_2 over a large portion of the solar spectrum [25]. Besides, it has exhibited higher photocatalytic performance than TiO_2 in some cases [26] and could take advantages of its comparatively lower manufacturing costs and higher lifetime and mobility of electrons [27]. In addition to photocatalytic applications, ZnO has been used in transducers, transparent ohmic contacts, transparent thin-film transistors, and optical devices [28].

Overall, due to their low cost and the possibility of generation of holes with high oxidizing power, both TiO_2 and ZnO could be considered ideal photocatalysts [27]. Despite the extensive efforts and enduring interest, photocatalysis technology suffers from the limitation to laboratory settings [6]. Suspended nanoparticles can provide high specific surface area, but with several drawbacks in the photocatalytic systems. For instance, the separation of nanoparticles after the wastewater treatment is required while it is expensive or toxic when discharged to the natural environment [29]. Moreover, the penetration depth of light could be restricted [29]. Furthermore, particle agglomeration can quickly reduce the effective surface area of the photocatalysts, leading to a rapid loss in photocatalytic performance [30]. In addition to photoactivity, it has been suggested that particle agglomeration can influence the light absorption as well [31]. Therefore, the immobilization of photocatalysts is considered an important strategy to overcome the drawbacks of suspended photocatalysis and facilitate the real-world applications of photocatalysis technology. Hence, up to now, various methods have been used to produce or modify the photocatalytic films and coatings comprising TiO_2 or ZnO [32–39]. There are different surface engineering techniques including chemical vapor deposition, physical vapor deposition, electroplating, sol-gel, ion beam-assisted deposition, electroless plating, thermal spraying, and laser surface engineering [40,41]. In general, as shown in Fig. 1, surface coating methods could be divided into three different groups of gaseous state, solution state, and molten/semi-molten state [40].

The applications of suspended TiO_2 and ZnO particles/nanoparticles in photocatalysis has been widely studied in the literature due the ease of using powders and their advantages such as high specific surface area. However, their practical applications are restricted due to some disadvantages, encouraging the vital role of surface engineering and coatings in photocatalysis technology. Notably, the application of thermal spraying and anodizing, as industrial surface engineering methods, in the fabrication of photocatalytic TiO_2 and ZnO coatings was studied in our previous work [26]. Hence, the application of some other surface engineering methods including physical vapor deposition (PVD) methods, dip coating, spin coating, spray coating/pyrolysis, and electrophoretic deposition (EPD) in the fabrication of TiO_2 and ZnO films for photocatalytic purposes is studied in this research to address the gap between laboratory experiments and practical applications of photocatalysis.

2. Characteristics of surface coatings

Surface engineering is the process of improving the surface properties of a material [42]. Usually, surface engineering methods constitute either compositional changes or microstructural modification or both [43]. Notably, thin films are layers of materials with thicknesses ranging from <1 nm to several μm [44], whereas thick films are layers with thicknesses typically ranging from 0.1 μm to 100 μm [45]. In order to evaluate the quality of coatings, several aspects including surface roughness, coating uniformity, volume porosity (pore size and pore distribution), thickness, and adhesion strength are important which are discussed in the following section.

2.1. Uniformity and surface roughness

The coating uniformity can be described by the consideration of different factors, and is generally given as a range which is not a precise value and is dependent of the number of data points [46]. Surface roughness is among important factors used to clarify the quality of post-manufacturing product [47]. Usually, five descriptors are used for the evaluation of the surface roughness of coatings that include R_t (distance between the highest peak and the lowest valley), R_z (distance

between the averages of five lowest valleys and the five highest peaks), R_v (distance between the lowest valley and the mean line), R_{pm} (distance between the mean line and the averages of five highest peaks), and R_p (distance between the mean line and the highest peak). It is noteworthy that R_{pm} and R_z are more reproducible [48].

2.2. Volume porosity

Volume porosity is another factor that can affect the photocatalytic activity [18]. Notably, development of nanostructured materials (to achieve large surface areas) and extension of porosity are popular approaches for improving the photocatalytic activity [49]. The creation of a large pore volume could facilitate the transport of products and reactants during photocatalytic process [50]. Moreover, it can increase the depth of light penetration into the photocatalytic material [51,52]. It has been stated that wide pore size distribution and large pore size could result in a higher photocatalytic activity [53].

2.3. Thickness

The effect of thickness on the photocatalytic activity of oxide semiconductor films has been researched. It has been suggested that increase of the thickness of the semiconductor films might remarkably improve the photocatalytic efficiency [54–59]. For instance, Xianyu et al. [59] have shown the higher photocatalytic activity of TiO_2 films (3.7 times) with 670 nm-thickness compared to that with 70 nm-thickness. In another research, Rivera et al. [55] evaluated the effect of thickness (50 nm–400 nm) on the photocatalytic activity of zinc oxide thin films deposited by RF magnetron sputtering where zinc oxide film with the thickness of 400 nm showed the highest photocatalytic activity for degradation of methylene blue. Notably, that apparent rate constant (k) of photodegradation of methylene blue significantly improved from 0.1444 h^{-1} to 0.6308 h^{-1} by an increase in the thickness from 50 nm to 400 nm. The higher photocatalytic activity of thicker coatings could be attributed to the greater amount of photo-generated e^-/h^+ pairs transferred from interior region to the surface of photocatalytic film [59]. However, it should be noted that thickness of coatings needs to be optimized since ultra-thick structures could suppress the photocatalytic performance [60,61].

2.4. Adhesion strength

Coating adhesion is very critical for many applications. Thus, several methods have been expanded to evaluate adhesion such as crosshatch and pill test [62], scratching the surface of coating [63], indenting the surface of coating [63], and pull-off method [64]. In general, the adhesion of coating to the substrate can be studied quantitatively or qualitatively that depends on the test method [63]. There are several factors that affect the coating adhesion strength which are mainly determined by the interfacial phenomena between the substrate and the coating. Moreover, microstructure properties (including residual stresses) could affect the coating adhesion [65]. Overall, the higher is the tensile residual stress within the coating, the lower is the adhesion of the coating [65,66]. In addition, the compressive stress within the coating could remarkably increase the coating adhesion [66]. Notably, it has been shown that presence of a controlled/optimized residual stress gradient in multilayer thin films could beneficially affect the adhesion of coatings [67]. Using high temperatures during the deposition process could accelerate diffusion at the interface of coating and substrate, leading to intermixing of the materials [65]. It is noteworthy that although photocatalytic coatings are not generally used in harsh conditions (under load and wear), using deposition methods which could provide higher adhesion strengths are preferred.

3. Vapor deposition methods

3.1. Physical vapor deposition

Physical vapor deposition is a common method used for the fabrication of coatings and could be easily combined with various methods to produce superior properties [68]. Besides, it has found numerous industrial applications [68]. PVD is an atomistic deposition process where vaporization of the solid or liquid source of the coating material leads to the formation of atoms/molecules in the vapor phase. Then, this vapor is transported to the surface of substrate through a vacuum or low pressure gaseous environment [69–71]. The vacuum environment could increase the mean free pass for collision between the substrate and vapor phase [72]. Finally, the complex condensation of vapor phase, using nucleation and growth processes, results in the formation of the coating. It is worth mentioning that PVD is a line of sight method [73]. Overall, this process involves four steps as follows [74]:

i. Evaporation of the coating material using a high energy source,
ii. Transport of the vapor to the surface of substrate,
iii. Reaction between the atoms and the reactive gas (during the last step), and
iv. Deposition of the film.

The individual steps could be responsible for stability and crystallinity of the deposited film [75]. This process can be used for deposition of elements, alloys, and compounds (by reactive deposition processes) [69]. The strong chemical bonding, which depends on the type of interface, could be responsible for high adhesion strength of coatings created by physical vapor deposition [65]. The way in which the energy is provided has resulted in the development of different deposition methods including sputtering, thermal evaporation, ion beam deposition, electron beam deposition, and pulsed laser deposition (PLD) [70] some of which are discussed in the following sections.

3.1.1. Thermal evaporation

Conventionally, thermal evaporation process is called vacuum deposition [76] and is specifically applicable for low melting point materials [77]. Thermal evaporation is considered a well-known method for producing a thin film where the source material is evaporated in a vacuum, facilitating the transfer of the vapor phase to a substrate where it is changed to a solid state again [77]. In the simplest case, an electrically heated tungsten wire around the source material can be used for thermal evaporation of elemental sources or compounds, e.g. metallization of silver or gold for electrical contacts [78]. Notably, thermal evaporation of metals with low to moderate deposition rates (10–100 nm min^{-1}) is considered one of the traditional PVD techniques that relies on the sublimation of the material onto a substrate (in vacuum) [79]. Resistive heating is the most common method used for evaporation of the material source (resistively heated boats or filaments are generally used for evaporation of the source material) [76]. Notably, graphite, zirconia, beryllia, alumina, quartz, and boron-nitride crucibles are indirectly heated [76]. A large direct current is applied to the resistive boat/coil to get the high melting points required for metals, and a high vacuum ($<10^{-4}$ Pa) supports the evaporation process and further transferring the vapor phase to the substrate [77]. Compounds could also be evaporated, but the process is more complex since their components are usually evaporated at different rates, requiring additional considerations [78]. One of the most important advantages of thermal vacuum evaporation, compared with spin coating, is the capability of fabrication of multi-layered films where the thickness of each layer could be easily adjusted [80].

Electron beam deposition is generally used for deposition of materials with high melting points, such as refractory metals, since they cannot be easily evaporated by the resistive heating [76]. Thus, it has been widely used for deposition of oxide semiconductors like TiO_2

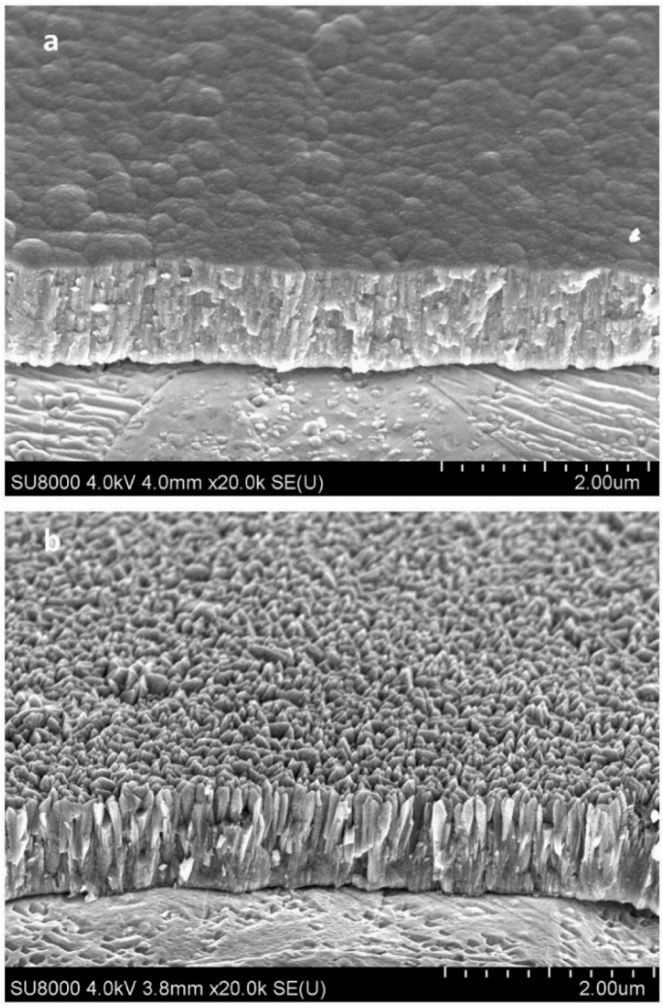

Fig. 2. SEM micrographs of the cross section of TiO_2 thin films deposited by electron-beam evaporation. Reproduced with permission from Ref. [89] Copyright 2016 Elsevier.

[81–84] and ZnO [85–87]. Duyar et al. [84] employed reactive electron beam evaporation for deposition of TiO_2 films, with thickness of 500 nm, using Ti_3O_5 as the starting material. The root mean square (RMS) roughness of the deposited films was in the range of 1.88–15.35 nm. They concluded that rougher surfaces could be formed with the increase of film thickness. Taherniya et al. [81] evaluated the effect of post annealing at 300, 450, and 600 °C, for 2 h, on the development of nanostructured anatase TiO_2 thin films prepared by electron-beam evaporation technique (with the thickness of 500 nm). Notably, the substrate temperature was kept at 150 °C during the deposition process. It has been shown that the as-deposited TiO_2 thin films were amorphous in structure. Although the crystallization of anatase phase was observed by post annealing at T = 450 °C, the complete crystallization was observed at T = 600 °C. It is worth mentioning that increasing the annealing temperature from 450 °C to 600 °C resulted in the increase of mean gain size from 12 nm to 24 nm. Besides, the porosity (i.e. the volume of pores per volume of coating) of titania films decreased from 40.68 % to 25.57 % by an increase in the annealing temperature from 450 °C to 600 °C. It is while the optical band gap energies did not change significantly. It should be noted that improvement of the structural properties of TiO_2 coatings generated by electron-beam evaporation followed by a post annealing heat treatment has also been reported by other researchers [88,89]. It has been stated that the deposited titania films using electron-beam evaporation are generally amorphous or consisted a mixture of amorphous and crystallite phases (mainly anatase) [88]. In general, anatase phase is the main crystalline phase formed by electron-beam evaporation (after post annealing heat treatment) as it has been reported by several researchers [89–93]. The SEM micrographs of the cross section of amorphous and crystalline (anatase) TiO_2 thin films deposited by electron-beam evaporation are shown in Fig. 2.

Notably, the faceted crystals were clear in the case of anatase TiO_2 thin film (with the grain size of around 100 nm at the surface). Thus, crystallization of TiO_2 thin films could result in the formation of a rougher surface compared with its amorphous structures [89]. Notably, anatase TiO_2 thin film deposited by electron-beam evaporation showed photocatalytic activity and superhydrophilic properties, whereas the amorphous one has showed neither photocatalytic activity nor superhydrophilic properties [89].

The same as TiO_2, the structural properties of ZnO coatings deposited by electron-beam evaporation could be improved using a post annealing heat treatment [94–96]. Although both zinc oxide films annealed at 400 °C and 600 °C were polycrystalline in nature, the one annealed at 600 °C showed better crystallinity and quality. However, using higher annealing temperature has resulted in the increase of the grain size [96]. Al Asmar et al. [95] also observed the same trend using a post annealing treatment at 550 and 750 °C temperatures (as-deposited ZnO thin film and ZnO thin films after post annealing process showed similar optical band gap energies, approximately). Increasing the substrate temperature, during electron-beam evaporation process, could increase both crystallinity and grain size of the deposited films. Notably, it has improved the transmittance of Al-doped ZnO electron-beam evaporated films which has been attributed to the higher crystallinity of the films fabricated at higher temperatures of the substrate [97]. On the downside, is has been shown that the quality of the electron-beam evaporated films depends on the type of substrate as the silicon (100) substrate resulted in a higher quality than glass substrate [96]. The dependency of the quality of ZnO thin films, produced by electron-beam evaporation, on the type of substrate or its temperature has also been reported by other researchers. Giri et al. [87] synthesized nanostructured ZnO thin films on glass substrates, alumina, and silicon substrates at different substrate temperatures using electron-beam evaporation method where ZnO thin films on silicon substrates at the temperature of 250 °C resulted in the highest quality. It is worth noting that the columnar growth along the c-axis was considered as the most favored orientation. A clear (002) orientation was observed for ZnO thin films created on glass and silicon substrates, signifying the columnar growth along the c-axis, whereas only a low intensity peak corresponding to (101) orientation was observed for ZnO thin films deposited on alumina substrate [87]. Overall, reactive electron-beam evaporation could be used as an efficient method for deposition of highly c-axis oriented ZnO thin films as it has been reported by several researchers [97–101]. The presence of oxygen (at the interstitial cites) is necessary for the formation of c-axis oriented ZnO thin films, and Gupta et al. [102] observed highly c-axis oriented ZnO thin films fabricated by sputtering unlike those produced by electron-beam evaporation. Increasing the thickness of films resulted in the formation of ZnO nanorods-like structures oriented normal to the substrate (with 50–100 nm diameter), whereas increasing the substrate temperature (at a constant thickness) led to the formation of crystalline morphology with granular structure (grain size of around 100 nm). It is notable that increasing the substrate temperature and thickness of coatings decreased the photoluminescence intensity [87] improving the photocatalytic activity of the films. On the downside, increasing the substrate temperature could decrease the deposition rate due to the probable decrease of attachment/adhesion of evaporated particles to the substrate as reported by Sahu et al. [97] for Al-doped ZnO (AZO) thin films fabricated by electron-beam evaporation. Another major drawback is that increasing the substrate temperature could result in the desorption of some species such as oxygen, changing the stoichiometry ratio between O and Zn, and deteriorate the crystallinity of the fabricated thin film, consequently [97]. Noteworthy, using post annealing treatment at

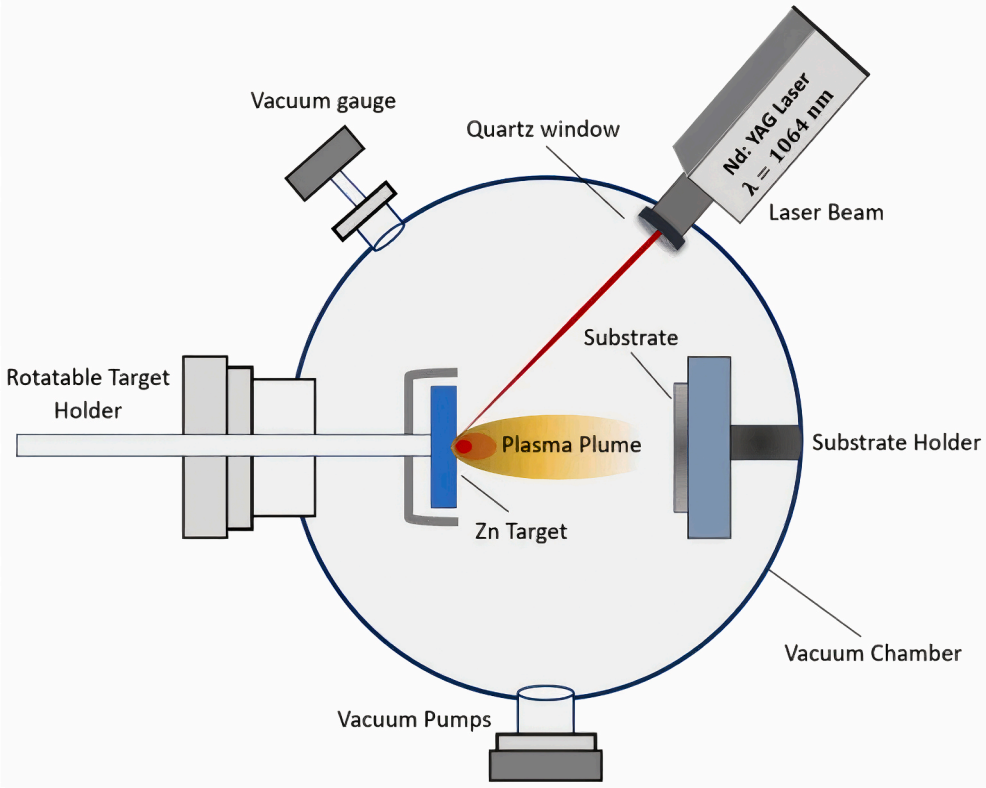

Fig. 3. Schematic illustration of a PLD system used to deposit ZnO film on porous silicon substrate. Reproduced with permission from Ref. [123] Copyright 2023 Springer Nature. The rights of this figure are owned by a third party.

high temperatures could lead to the conversion of the surface morphology of ZnO thin films from columnar grains to relatively flat surfaces (in addition to the increased grain size). Moreover, it can reduce the surface roughness of the photocatalytic thin films [96]. It is worth mentioning that increasing the substrate temperature, during the electron-beam evaporation process, could also decrease the surface roughness and provide smother films which can be attributed to the increased energy of the ejected particles [97]. Substrate temperature could significantly affect the diffusion and hopping distance and therefore, the adatoms could be cooled down slower and their diffusion length becomes larger by increasing the substrate temperature, leading to the formation of smoother thin films, finally [97]. Overall, it can be concluded that the morphology (surface roughness, width, and height of nano-columnar structures), photo-absorption ability, and grain size of the deposited thin films using electron-beam evaporation remarkably depends on the thickness of film, type of the substrate and its temperature. Falcao et al. [103] used two different processes including plasma deposition (PD) and electron-beam evaporation with plasma assistance (EBPA), in an argon atmosphere, for fabrication of ZnO thin films. Plasma has been used for sublimation of the source material offering several advantages such as economical/efficient usage of the raw material, large area deposition, low ion damage, and low temperature deposition. Although the refraction index of ZnO film fabricated by plasma deposition was 2.07 which is close to that of pore-free wurtzite (i.e. 2.0), signifying the good quality of the film, electron-beam evaporation resulted in the fabrication of ZnO film with a smaller index of refraction (i.e. 1.87) compared with that of pore-free wurtzite clarifying the less dense nature of ZnO thin film produced by EBPA than that deposited by PD. Notably, both EBPA and PD methods led to the fabrication of strongly c-axis oriented ZnO thin films which has been attributed to the low temperature of substrate favoring the growth of (002) planes owing to their low surface energy. However, the band gap energy of ZnO film produced by PD (i.e. 3.10 eV) was narrower than that of fabricated by EBPA (i.e. 3.15 eV). It can be attributed to the larger density of defects in PD films which was confirmed by the higher carrier concentration of PD film than EBPA film (carrier concentration of undoped ZnO films could be controlled by defects including interstitial Zn ions and/or oxygen vacancies). On the downside, EBPA film showed much higher mobility than PD film, ca. 2.2 times, which has been attributed to the much higher carrier concentration of PD film.

3.1.2. *Sputtering*

The deposition of particles vaporized from a target using physical sputtering is called sputter deposition [69]. In physical sputtering, the surface atoms of the target material are ejected physically by the transfer of momentum from an energetic bombarding particle (atomic-sized) which is generally a gaseous ion (accelerated from a plasma) [69]. Magnetron sputtering is considered the most common process to grow thin films where positively charged ions bombard the target in the plasma of a magnetically enhanced glow discharge [104]. Generally, a radiofrequency (RF) source or a DC source are used for the generation of plasma [105]. Owing to its several advantages, magnetron sputtering is considered a leading coating technology to produce functional films [106]. Unlike DC excitation which can be applied only to conductive targets, RF excitation can be applied to either nonconductive or conductive targets [105]. Ion beam sputtering is another approach in which an ion source is used for generation of a focused ion beam on the target material. To assist the deposition by bombarding the growing film, a second ion gun can be used to improve density, adhesion, and control of the stoichiometry. Bombardment using a low-energy reactive ion beam could enhance the rate of compound formation [107]. The advantage of plasma and ion beam sputtering is the potential control of the contamination using a high pumping speed and a good vacuum, but ion beam sputtering could suffer from its relatively high cost [108]. Magnetron sputtering takes advantages of a magnetic field around the target material to energize bombarding atoms. Such a magnetic field

Table 1
Application of PLD for the deposition of photocatalytic TiO_2 and ZnO films.

Photocatalytic film	Thickness	Pollutant (concentration)	Source of light	Efficiency	Reference
Anatase TiO_2	~10–20 nm	Methyl orange (NA)	UV	48 % (t = 5 h)**	[128]
Rutile TiO_2	100 nm	Methylene blue (1 mg L^{-1})	UV	16 % (t = 2.5 h)*	[129]
Anatase TiO_2	60 nm	Methylene blue (1 mg L^{-1})	UV	22 % (t = 2.5 h)*	[129]
Rutile TiO_2	160 nm	Methylene blue (1 mg L^{-1})	UV	26 % (t = 2.5 h)*	[129]
Anatase TiO_2	150 nm	Methylene blue (1 mg L^{-1})	UV	39 % (t = 2.5 h)*	[129]
Rutile TiO_2	~10–20 nm	Methyl orange (NA)	UV	73 % (t = 5 h)**	[128]
N-doped TiO_2	NA	Methyl orange (2 mg L^{-1})	Visible	100 % (t = 4 h)**	[130]
ZnO	NA	Rhodamine B (0.1 % - mass to volume)	Sunlight	90 % (t = 6 h)**	[131]
ZnO (grown on c-plane sapphire)	~270 nm	Rhodamine B (~10 mg L^{-1})	Xe lamp (full arc)	74 % (t = 1 h)**	[132]
ZnO (grown on a-plane sapphire)	~270 nm	Rhodamine B (~10 mg L^{-1})	Xe lamp (full arc)	57 % (t = 1 h)**	[132]

Note: * (Contribution of degradation and adsorption) - ** (Contribution of degradation).

could trap electros around the target improving plasma. It leads to the higher ionization of bombarding atoms, therefore, the bombarding rate and the deposition rate increase [109]. Compared with non-magnetron sputtering, magnetron sputtering could remarkably increase the deposition rate from 0.1 nm min^{-1} to 20 nm min^{-1} [110]. Unlike TiO_2 films produced by electron-bean evaporation, the rutile phase is generally observed in the films provided by magnetron sputtering [88]. Refractive index is defined as the ratio of the speed of light in air or vacuum to that in a transparent material [111]. Preparation conditions affect the refractive index of films and coatings since it could be dependent on the crystal structure, the faction of voids (and/or mass density), the relative values of grains and/or crystallite size, and the surface roughness, e.g. Yao et al. [88] showed that the refractive indices of TiO_2 films deposited by electron-beam evaporation and reactive magnetron sputtering processes were 2.30 and 2.50, respectively. Notably, on the condition of similar operating conditions, using sputtering method instead of electron-beam evaporation process could not significantly affect the optical bend gap energy, surface texture, and surface roughness of the films as reported by Al Asmar et al. [95] Reactive sputtering is considered another form of sputter deposition. In such a process, a reactive gas (such as nitrogen or oxygen) is mixed with the sputtering agent (such as argon gas) to form special compounds [112,113]. Reactive magnetron sputtering has been widely used for the deposition of oxide films including TiO_2 [114,115] and ZnO [116,117].

Evaporation and sputtering are the most common PVD processes [71]. PVD processes can be used for the deposition of thin and thick films with the thickness ranging from a few to thousands of nm [118]. Notably, sputtering processes could result in denser and more compacted films than those prepared by evaporation processes (due to the incident momentum) [105]. Besides, the low temperature of target could provide the possibility of deposition of oxide semiconductors which could be decomposed at high temperatures (as encountered in evaporation processes) [105]. Moreover, sputtering process is more versatile than evaporation methods. Thus, it has been widely used for industrial applications (since plasma sources and targets can be constructed in different shapes for various configurations) [105].

3.1.3. *Pulsed laser deposition*

Pulsed laser deposition or laser ablation is among PVD processes (performed in a vacuum system) that shares some process characteristics with sputtering and some with molecular beam epitaxy [119]. In this process, an intense laser beam (such as Nd-YAG, UV, excimer, and Ti-Sapphire) at different pulse rates, from near-continuous to femtosecond, is focused on the target to evaporate, ablate, and/or exfoliate the material [120,121]. The extremely short pulse duration (picosecond and femtosecond regime) could reduce/prevent thermal damage. Besides, it can lower threshold fluences of ablation (unlike conventional nanosecond regime) [120]. Stoichiometry of the deposited films mainly depends on some operational parameters such as distance of the target to the substrate and laser fluence (apart from the chemical composition of the target) [122]. To provide high density of laser energy, tiny amount of the target material is ablated resulting in a plasma plume containing different energetic species such as molecules, ions, particles, atoms, molten globules, clusters, and electrons [119,121]. Schematic illustration of a PLD system to fabricate ZnO film on porous silicon substrate is shown in Fig. 3.

The growth of layer mainly depends on condensing plasma fluxes (particle energy, density, degree of ionization, and spatial distribution) and the substrate properties (activation energy of surface desorption, density of adsorption sites, and temperature) [119]. PLD can be used for deposition of high-quality/high-purity single-component and multi-component thin films [124–126]. Moreover, it can be used for deposition of single-layer or multi-layered films for both single-component and multi-component materials [127]. Generally, this method is more favorable than sputtering for stoichiometric deposition of complex compounds [105]. Owing to its unique properties, PLD has been widely used for the fabrication of TiO_2 and ZnO coatings for photocatalytic purposes, as provided in Table 1.

Yamaki et al. [133] deposited epitaxial TiO_2 thin films on (0001) sapphire substrates for the photocatalytic degradation of methylene blue. The deposited films were mainly composed of rutile phase (with small amount of anatase phase). It has been shown that using lower laser fluence not only could increase the ratio of anatase to rutile phases, but also could fabricate rougher surfaces consisting of coarse grains. Thus, the TiO_2 thin film deposited using the laser fluence of 50 mJ showed the highest photocatalytic activity than those deposited using laser fluences of 100, 150, and 200 mJ. It is worth mentioning that the substrate material can affect the growth mechanism of TiO_2 thin films deposited by PVD processes [134]. Notably, $SrTiO_3$ (001) or $LaAlO_3$ (001) substrates have been extensively used for the deposition of anatase TiO_2 (001) epitaxial thin films in pulsed laser deposition [135–138], whereas some other substrates (such as Al_2O_3) have been generally used for the deposition of rutile TiO_2 (011) epitaxial thin films [139]. It is also possible to deposit pure anatase and rutile phases on a specified substrate (such as Al_2O_3) by changing only the annealing and growth conditions [140,141]. In PLD method, the ratio of anatase to rutile could depend on the pressure of system [142], substrate temperature, and laser repetition rate/frequency [143]. Inoue et al. [143] showed that although anatase phase could be formed at low temperatures (i.e. 150 °C), regardless of the repetition rate, increasing the repetition rate could induce the formation of anatase phase at high temperatures (i.e. 300 °C). They suggested that PLD could be advantageous for deposition of high quality TiO_2 thin films using specific control of time-dependent temperature. Substrate temperature could also affect the type of growth (random or oriented). Although Zhao et al. [144] observed the stability of anatase phase by increasing the substrate temperature from 500 °C to 800 °C, the anatase structure changed from random-growth to oriented-growth after 600 °C. Notably, the random structure of anatase phase, deposited at 600 °C, showed higher photocatalytic activity than its (211)-oriented structure (deposited at 800 °C) which could be attributed to the lower band gap energy and smaller average nanometer particle size at lower substrate temperatures. Luttrell et al. [128]

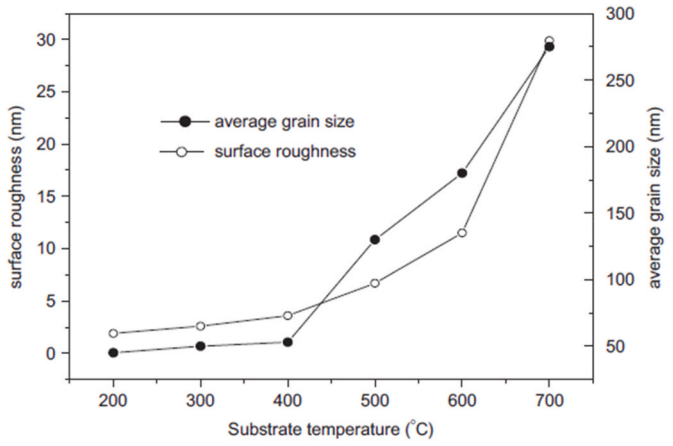

Fig. 4. Effect of substrate temperature on the average grain size and surface roughness RSM of ZnO thin films deposited by PLD. Reproduced with permission from Ref. [147] Copyright 2007 Elsevier.

synthesized anatase and rutile TiO_2 epitaxial thin films on $LaAlO_3$ and Al_2O_3 substrates, respectively, to compare the photocatalytic activity of pure anatase and rutile phases where, the as-grown anatase films were approximately twice as active as the rutile films for the photocatalytic degradation of methyl orange under UV illumination. To evaluate the effect of temperature and pressure on the topography (surface roughness) of thin films deposited by PLD, Lin et al. [142] deposited TiO_2 at two different temperatures of 873 K and 1073 K and at two different pressures of 33 Pa and 100 Pa. RSM roughness values for TiO_2 thin films deposited at different conditions of T = 873 K and P = 33 Pa, T = 873 K and P = 100 Pa, T = 1073 K and P = 33 Pa, and T = 1073 K and P = 100 Pa were 8.4, 11.2, 47.2, and 50.6 nm, respectively. As it can be seen, unlike pressure, deposition temperature could significantly affect the surface roughness of TiO_2 films deposited by PLD method. In another research, Hu et al. [130] deposited N-doped TiO_2 by pulsed laser deposition for the photocatalytic degradation of methyl orange under visible-light irradiation. Although they showed that anatase N-doped TiO_2 could be fabricated at both room temperature and higher temperatures (200 °C and 400 °C), the deposited films at higher temperatures showed a significantly higher photocatalytic activity which has been attributed to the higher crystallinity (accompanied by increasing the grain size), surface roughness, and visible-light absorption of the deposited thin films at higher temperatures. Overall, the photocatalytic activity of titania films deposited by PLD is dependent on the substrate properties including its temperature.

PLD has also been used to deposit ZnO films. Mosnier et al. [145] deposited ZnO film (thickness = 2 μm) on a soda lime glass substrate at room temperature. The as-deposited film was highly textured with the orientation of wurtzite (0002), c-axis perpendicular to the surface of ZnO film, with the RMS roughness of 49.7 nm. Yudasari et al. [131] deposited wurtzite ZnO thin films on glass substrates at room temperature for the photocatalytic degradation of Rhodamine B under sunlight irradiation. The nanostructured ZnO thin film showed preferred orientation along (100), (002), and (101). Fabrication of wurtzite ZnO films with different orientations (despite of using glass substrates at room temperature in both cases) [131,145] clarifies dependency of ZnO films on deposition conditions which is consistent with the results achieved by TiO_2 films (as discussed previously). He et al. [146] evaluated the effect of substrate temperature on the quality of ZnO films on Si substrates deposited by PLD. It has been shown that increasing the substrate temperature, up to 600 °C, could improve the crystallinity of the deposited films. Besides, more uniform textured ZnO films (i.e. grains with c-axes perpendicular to the surface of substrate) were formed at higher temperatures (up to 600 °C). Zhao et al. [147] evaluated the effect of substrate temperature on ZnO thin films deposited on sapphire substrates, where all wurtzite ZnO films were highly textured (c-axis-oriented). Effect of substrate temperature on the average size and the surface roughness of ZnO thin films deposited on sapphire substrates are shown in Fig. 4.

As shown, increasing the substrate temperature enhanced both average grain size and surface roughness RSM though at varying degrees [147]. It is obvious that the effect of substrate temperature on the surface roughness was more than that on the grain size. Abdell-Fattah et al. [148] evaluated the effect of both substrate temperature and laser fluence effects on the quality of nanostructured ZnO this films deposited on glass substrates by PLD. Irrespective of the laser fluence, polycrystalline wurtzite ZnO thin films were deposited at low temperatures (25 °C). Whereas, increasing the substrate temperature led to the formation of textured ZnO thin films (c-axis orientation) through acceleration of the diffusion of Zn and O atoms to more favorable positions (energetically). It is worth mentioning that increasing the substrate temperature increased the crystallites size of ZnO thin films, whereas increasing the laser fluence decreased the crystallite size. However, it has been shown that increasing the substrate temperature significantly improved the quality of ZnO thin films, while, increasing the laser fluence slightly affected the quality of films [148], clarifying the crucial effect of substrate temperature on the quality of ZnO thin films. Notably, unlike laser fluence, increasing the substrate temperature from 25 °C to 300 °C did not significantly affect the RMS roughness. It is also worth mentioning that decreasing the laser fluence from 4 J cm^{-2} to 2.37 J cm^{-2} remarkably increased the RMS roughness from 0.4 nm to 0.7 nm [148]. Li et al. [132] demonstrated the key role of surface roughness and photo-absorption ability in the photocatalytic activity by deposition of oriented (002) ZnO thin films on a-face and c-face sapphire (using PLD). Although ZnO thin film deposited on a-face sapphire (i.e. ZnO(a)) showed a higher crystallinity than that deposited on c-face sapphire (i.e. ZnO(c)), ZnO(c) showed a higher photocatalytic activity which could be related to the significantly higher surface roughness of ZnO(c) at 8.6 nm

Table 2
Advantages and disadvantages of PVD processes.

Advantages [74,118,157]
a) All inorganic and some organic materials can be used as coating materials.
b) Both multi-layered and mono-layered coatings could be deposited using this method.
c) It can be used for deposition of graded composition coatings.
d) Thick films could be obtained using this method.
e) Continuous variation of the characteristics of coating could be provided.
f) It has adaptability and flexibility to market demands.
g) It is known as an environmentally-friendly process.
Disadvantages [74,158]
a) It cannot be easily used for complex shapes.
b) It has a high process cost.
c) It suffers from low output.
d) It generates smoother surfaces compared with some other surface engineering processes.
e) It is considered a complex process.

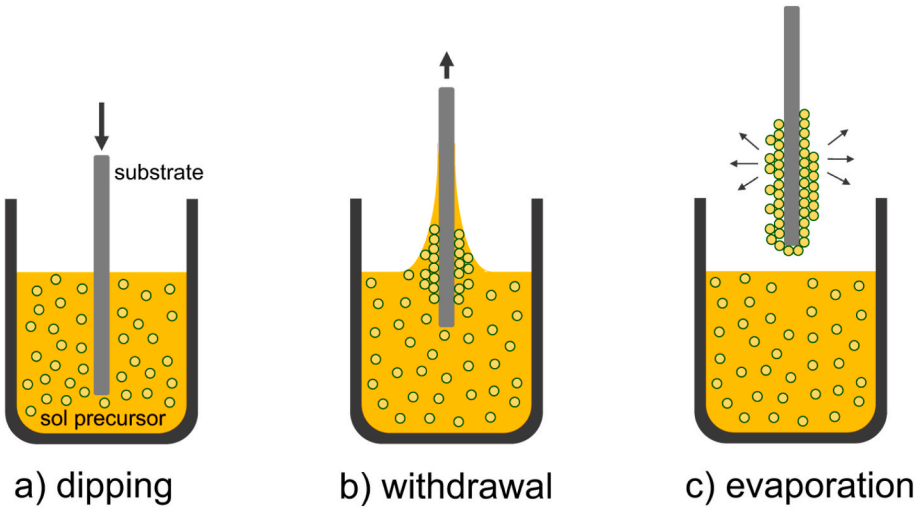

Fig. 5. Sequential stages of dip coating procedure. Reproduced with permission from Ref. [172] Copyright 2022 Springer Nature. The rights of this figure are owned by a third party.

than ZnO(a) at 1.1 nm, and its higher photo-absorption ability. Overall, PLD can take advantages of several features including high adhesion, absence of pores and contamination, fast response, using various forms of the target material (single crystal, powder, and sintered pellets) energetic evaporation, stoichiometric transfer of target material to the substrate (congruent evaporation), capability of using both reactive and inert gas deposition (flexibility), capability of using different kinds of substrates, and a wide range of operational temperature and pressure [76,142,149–151]. Although the absence of pores is an important advantage in some applications such as wear-resistant coatings [152,153], the presence of pores (up to an optimum amount) could improve photocatalytic activity by increasing surface area. On the downside, PLD has from some drawbacks such as relatively high cost that is mainly attributed to the lasers (specially for picosecond and femtosecond pulsed lasers) which has made it far away from widespread use in industrial/laboratorial applications [154]. In addition, it suffers from the non-uniformity of coatings and the formation of micrometer-sized particles during the deposition process (which cannot be eliminated completely) [155]. Reduction of the energy density of pulsed laser could reduce or eliminate the formation of micrometer-sized particles, however, it lowers the deposition rate [156]. Notably, using hybrid methods (for example combination of magnetron sputtering and pulsed laser deposition) could result in improving the quality of deposited films and increasing the deposition rate and the uniformity of films [156]. PLD has also a narrow forward distribution which makes it a difficult task to be used for large area scale-up [151], but using off-axis PLD is considered a promising solution to overcome this problem [122].

Overall, there are several advantages and disadvantages over using PVD processes, which are provided in Table 2.

4. Liquid deposition methods

4.1. Dip coating

Dip coating is generally used for the production of functional films [159]. It is a facile and economical process in which the substrate is immersed into the solution of the coating material, and is withdrawn from the solution tank after being fully infiltrated [160]. Dip coating could be known as slurry or vacuum slurry dip coating. The slurry is composed of dispersant, ceramic particles, binder, and solvent where the thickness and smoothness of the film could be adjusted by modification of the draw-up speed of the substrate from the slurry and the solid loads in it [159]. Sol-gel process as an inexpensive and simple technology could also be used for the fabrication of oxide films [161]. Using a solution containing the source compounds of the target material is the basis of most sol-gel processes. The solution changes into a sol by the formation of fine colloidal particles/polymers. Further reactions could result in the formation of a wet gel (gelation) and coating is made during sol-to-gel conversion. Usually, the target material is obtained by the heat treatment of the shaped gel at high temperatures [162]. Sol-gel is known as a cost effective, non-vacuum, environmentally-friendly, and clean process that possesses low requirements for the substrates and good chemical homogeneity [163–166]. Low cost could be considered the most important reason for the widespread use of sol-gel coatings, however, sol-gel coatings could suffer from their delamination [167]. Overall, sol-gel method could be used by a range of coating methods including dip coating, spray coating, and spin coating [168]. Dip coating is defined as the process of deposition of a solid film on a substrate which is immersed in a solution (or sol) followed by withdrawal and drying. It

Table 3
General advantages and disadvantages of dip coating.

Advantages [46,169–171,173]
a) Wide operating range
b) Ease of run
c) Deposition of hybrid, nanocomposite, and inorganic materials
d) Inexpensive hardware
e) Exploitation of the purity of solution chemistry (such as sol-gel method)
f) Easily adjustable layer thickness
g) Capability of large-scale application for products with low standard requirements
h) Capability for coating items with various complex surfaces (with intricate shapes and holes)
Disadvantages [174]
a) Lack of uniformity of the coatings
b) High sintering temperatures (>1000 °C) for non-organic coatings, resulting in the creation of defects in metals.

Table 4
Application of dip coating process for deposition of photocatalytic TiO_2 and ZnO films.

Photocatalytic film	Thickness	Pollutant (concentration)	Source of light	Efficiency	Reference
TiO_2	NA	Methyl orange (0.015 mM)	UV	68.5 % (t = 5 h)	[175]
TiO_2	NA	Methyl orange (0.03 mM)	UV	39.9 % (t = 5 h)	[175]
TiO_2	NA	Methyl orange (0.045 mM)	UV	23.1 % (t = 5 h)	[175]
TiO_2	NA	Methyl orange (0.06 mM)	UV	20.4 % (t = 5 h)	[175]
N-doped TiO_2	NA	Methylene blue (5 mg L^{-1})	Visible	52 % (t = 210 min)**	[176]
N-doped TiO_2	NA	Methylene blue (5 mg L^{-1})	UV	60 % (t = 210 min)**	[176]
N-doped TiO_2	NA	Eriochrome black-T (5 mg L^{-1})	Visible	31 % (t = 210 min)**	[176]
N-doped TiO_2	NA	Eriochrome black-T (5 mg L^{-1})	UV	41 % (t = 210 min)**	[176]
TiO_2	Estimated to be ~150–200 nm	Toluidine (5×10^{-4} M)	Visible	24 % (t = 8 h)**	[177]
N-doped TiO_2	Estimated to be ~150–200 nm	Toluidine (5×10^{-4} M)	Visible	45 % (t = 8 h)**	[177]
Li-doped TiO_2	Estimated to be ~150–200 nm	Toluidine (5×10^{-4} M)	Visible	55 % (t = 8 h)**	[177]
Li-N co-doped TiO_2	Estimated to be ~150–200 nm	Toluidine (5×10^{-4} M)	Visible	61 % (t = 8 h)**	[177]
N-doped TiO_2	Estimated to be ~150–200 nm	Aniline (5×10^{-4} M)	Visible	77 % (t = 7 h)**	[177]
N-doped TiO_2	Estimated to be ~150–200 nm	Dimethylaminopyridine (5×10^{-4} M)	Visible	65 % (t = 7 h)**	[177]
N-doped TiO_2	Estimated to be ~150–200 nm	Methylbenzylamine (5×10^{-4} M)	Visible	60 % (t = 7 h)**	[177]
Li-N co-doped TiO_2	Estimated to be ~150–200 nm	Aniline (5×10^{-4} M)	Visible	88 % (t = 7 h)**	[177]
Li-N co-doped TiO_2	Estimated to be ~150–200 nm	Dimethylaminopyridine (0.0005 M)	Visible	78 % (t = 7 h)**	[177]
Li-N co-doped TiO_2	Estimated to be ~150–200 nm	Methylbenzylamine (0.0005 M)	Visible	67 % (t = 7 h)**	[177]
ZnO	218 nm	Methylene blue (1×10^{-5} M)	UV	73 % (t = 4 h)	[178]
ZnO	312 nm	Methylene blue (1×10^{-5} M)	UV	69 % (t = 4 h)	[178]
ZnO	437 nm	Methylene blue (1×10^{-5} M)	UV	63 % (t = 4 h)	[178]
ZnO	Order of 100 nm	Methylene blue (2.5×10^{-5} M)	UV	90 % (t = 10 h)	[179]
Al-doped ZnO	150 ± 20 nm	Methylene blue (2.5×10^{-5} M)	UV	80 % (t = 380 min)**	[180]
ZnO	150 ± 20 nm	Methylene blue (2.5×10^{-5} M)	UV	60 % (t = 380 min)**	[180]
ZnO	NA	Methylene blue (1×10^{-5} M)	UV	66 % (t = 4 h)	[181]
ZnO	NA	Rhodamine B (1×10^{-5} M)	UV	69 % (t = 4 h)	[181]
ZnO	NA	Reactive orange (1×10^{-5} M)	UV	33 % (t = 4 h)	[181]
Ag-doped ZnO (1 mol%)	NA	Methylene blue (1×10^{-5} M)	UV	67 % (t = 4 h)	[181]
Ag-doped ZnO (3 mol%)***	NA	Methylene blue (1×10^{-5} M)	UV	69 % (t = 4 h)	[181]
Ag-doped ZnO (5 mol%)	NA	Methylene blue (1×10^{-5} M)	UV	73 % (t = 4 h)	[181]
Ag-doped ZnO (7 mol%)	NA	Methylene blue (1×10^{-5} M)	UV	75 % (t = 4 h)	[181]
Ag-doped ZnO (10 mol%)	NA	Methylene blue (1×10^{-5} M)	UV	79 % (t = 4 h)	[181]
Ag-doped ZnO (10 mol%)	NA	Rhodamine B (1×10^{-5} M)	UV	79 % (t = 4 h)	[181]
Ag-doped ZnO (10 mol%)	NA	Reactive orange (1×10^{-5} M)	UV	49 % (t = 4 h)	[181]

Note: ** (Contribution of degradation).
Note: *** (The values reported in this study for element doping or the contribution of a material in a composite might be nominal and may not accurately reflect the exact concentrations in some cases).

has been stated that big/complex shapes, such as cylinder tubes, could be coated using a one step process, while such a simplicity is not always possible by using evaporative/sputtering methods [169]. The main forces that play important roles in dip coating process are inertia force, gravitational force, viscous drag, and surface tension [170]. Overall, it consists of five separate steps as follows [171]:

1 Immersion: In the first step the substrate is dipped, using a constant speed, into the sole or colloidal solution of the coating material (a pretreatment process could be required which depends on the type of substrate).

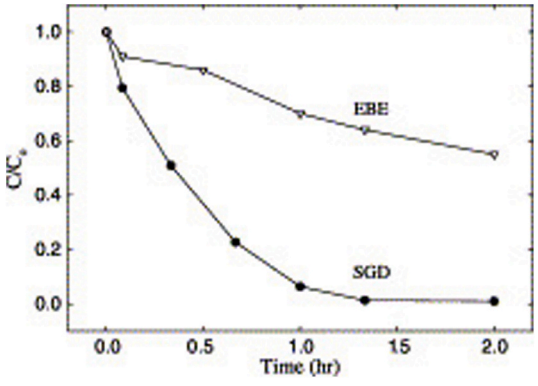

Fig. 6. Comparison of the photocatalytic activity of TiO_2 thin films deposited by SGD and EBE processes. Reproduced with permission from Ref. [82] Copyright 2003 Elsevier.

2 Startup: In the second step, the substrate should be kept in the sol or the coating solution for a designated time and should be pulled out afterward.
3 Deposition: In this step, the coating material or the sol is deposited on the substrate while it is being pulled out. The removal speed can significantly affect the thickness of the coating (a slower speed could result in a thinner layer).
4 Drainage: In the fourth step, excessive liquid should be drained from the surface of the substrate.
5 Evaporation: In the last step, solvent should be evaporated from the substrate surface to form a coating. Notably, this step might be carried out in step three if the solvent is volatile.

Schematic illustration of dip coating process is shown in Fig. 5, and its major advantages and disadvantages are provided in Table 3.

General operating parameters of dip coating process are as follows [46]:

- Wet thickness: 10–200 μm,
- Coverage uniformity: ±10 %,
- Viscosity: 20–2000 cP, and
- Line speed: 0.5–7.5 m s^{-1}

Due to simplicity and low cost, it has received remarkable attention for deposition of different kinds of semiconductors, including TiO_2 and ZnO, for photocatalytic applications (Table 4).

As shown, this method could take advantage of deposition of ZnO and TiO_2 films with a variety of thicknesses from hundreds of nanometers (30 nm) to several micrometers (5 μm). Oh et al. [82] deposited TiO_2 thin films on soda lime glass substrates using both electron-beam

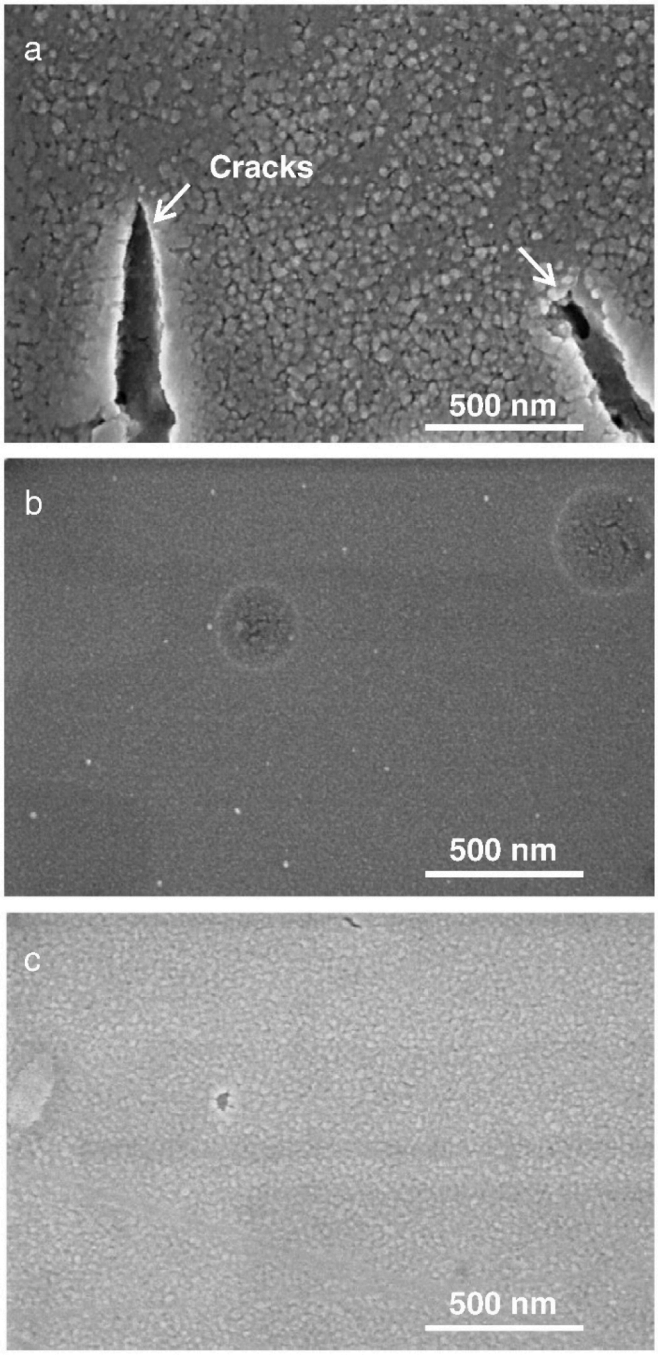

Fig. 7. SEM micrographs of TiO_2 films. (a) TiO_2/SLG, (b) TiO_2/BSG, and (c) TiO_2/QS after calcination at 450 °C. Reproduced with permission from Ref. [182] Copyright 2011 Elsevier.

evaporation (EBE) and sol-gel dip coating (SGD) processes. Thickness of the deposited films were around 400 nm. The deposited films were calcined at different temperatures, from 300 °C to 500 °C, and used for the photocatalytic degradation of formic acid under UV irradiation. Upon heating at 500 °C, the refractive index of TiO_2 films deposited by EBE insignificantly increased from 2.09 to 2.13, whereas the refractive index of TiO_2 films deposited by SGD increased from 1.79 to 1.93. Besides, increasing the calcination temperature resulted in a decrease of porosity from 58.8 % to 49.1 % and from 37.1 % to 33.9 % for SGD and EBE films, respectively. Obviously, dip coating resulted in the formation of photocatalytic coatings with higher porosity than those deposited by electron-beam evaporation. Notably, XRD patterns confirmed the formation amorphous TiO_2 thin films even after calcination at 300 °C (for both EBE and SGD methods), signifying the necessity of using calcination at high temperatures for the creation of crystalline structures. The photocatalytic activity of titania films deposited by EBE and SGD methods is compared in Fig. 6.

As evident, the TiO_2 film deposited by SGD showed a remarkably higher photocatalytic activity than that deposited by EBE. The higher porosity of SGD films and the formation of Ti^{3+} ions (due to the reduction of Ti^{4+} to Ti^{3+} by organic residues) during the calcination of SGD films resulted in their higher photocatalytic activity than EBE films [82]. Ghazzal et al. [182] deposited TiO_2 thin films using dip coating process on soda-lime glass (SLG), borosilicate glass (BSG), and quartz substrates (QS). SEM micrographs showed the presence of some cracks in the dip-coated TiO_2 film on the soda-lime glass substrate as shown in Fig. 7 (unlike those deposited on borosilicate and quartz substrates).

Significantly different thermal expansion coefficient between TiO_2 film and soda-lime glass substrate could play a vital role in the appearance of these cracks. Dehydration of water from titania film, during the calcination step, could also result in the formation of cracks. It is notable that anatase phase with preferential (101) orientation was observed for all deposited films [182]. Hence, the quality of photocatalytic films deposited by dip coating may highly depend on the substrate properties. Despite of its advantages, dip coating process could also suffer from the slow rate of process [170] and the non-uniformity of film thickness [183].

4.2. Spin coating

Spin coating is one of the well-known methods for deposition of oxide semiconductors including TiO_2 and ZnO [184–187]. Notably, it is a common method to provide homogeneous and uniform thin films where a tiny amount of the solution of coating material is placed on the substrate which is spun for a specific time (as high speed); and each layer of the film is dried by evaporation of the solvent before starting the next coating layer [188]. Thickness of the film can be controlled by spinning velocity, solution viscosity, and surface tension [189]. In general, this process consists of some sequential stages including fluid dispense, spin up, stable fluid outflow, and evaporation [190]. Schematic illustration of spin coating is shown in Fig. 8.

Hence, the material is firstly deposited on the turntable. Then spin up and spin off processes take place sequentially. It is notable that the evaporation happens during the process [192]. Flow-controlled and evaporation-controlled are the stages that could play the most important role in the final thickness of coatings. Overall, fluid flow on a flat substrate is an important physical process in spin coating [193]. Moreover, high spinning speed could lead to the formation of thinner layers [192]. Spin coating results in the formation of an amorphous phase, necessitating the use of high temperatures for crystallization of the deposited films [194]. The main processing parameters of this method of deposition include solution concentration, solution viscosity, spin speed, dispense volume, spin time, and film thickness. Notably, this process could provide coatings with a wide range of thickness up to 200 μm [193]. Pore and surface characteristics of the substrate could affect that quality of the deposited film [195]. It is noteworthy that high-temperature thin-film processing could introduce major difficulties in combining the desirable crystalline thin films with unstable substrates at elevated temperatures. Moreover, it is a significant cost to manufacturing [194]. Major merits and drawbacks of spin coating are summarized in Table 5.

Overall, spin coating has received potential attention for deposition of different kinds of ceramic materials, including TiO_2 and ZnO, for photocatalytic applications some of which are tabulated in Table 6. Notably, nitrogen doping resulted in the improvement of the photocatalytic activity of TiO_2 film deposited by spin coating process [198]. Fe^{3+} [199], Co^{2+} [200], and Ag^{2+} [201] doping also improved the photocatalytic activity of TiO_2 and ZnO spin coated thin films which

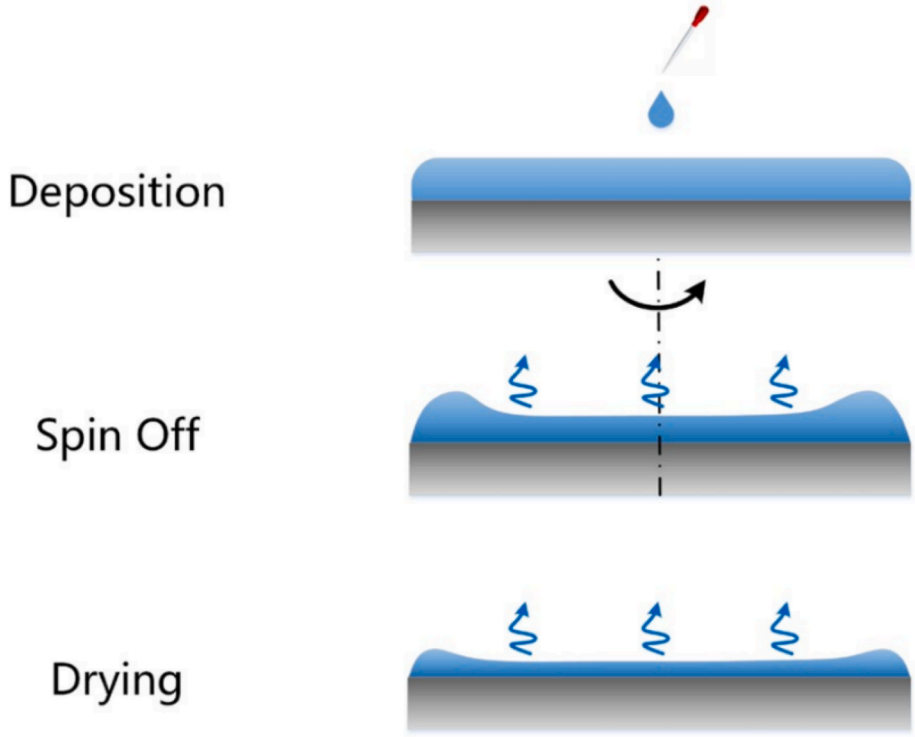

Fig. 8. Schematic illustration of spin coating. Reproduced with permission from Ref. [191] Copyright 2021 MDPI. This article is an open access article distributed under the terms and conditions of the Creative Commons Attribution (CC BY) license (https://creativecommons.org/licenses/by/4.0/).

Table 5
General merits and drawbacks of spin coating.

Advantages [170,189,193,196,197]
a) Possibility of deposition of different types of materials including polymers and nanoparticles
b) The simplest method for the deposition of films
c) Low cost
d) Easy control of thickness (by switching to a different viscosity photoresist or changing the speed of spin)
e) Uniform coating (specially for thin films)
f) Very fast process
Disadvantages [170,190,192,197]
a) Necessity of using a drying or baking process
b) Creation of relatively planar surfaces
c) Sensitivity to environmental conditions
d) Limited size of the substrates
e) Coating material loss (95–98 % of material is flung off)
f) Difficulty of creation of multilayered structures (more than two layers)
g) Possibility of the presence of contaminants (humidity, solvent, etc.)

could be attributed to the trapping effect of photo-generated e^-/h^+ pairs. It is while, both Cu^{2+}-doping and Fe^{3+}/Cu^{2+} co-doping adversely affected the photocatalytic activity of anatase TiO_2 [202] since dopants, on the downside, could act as recombination centers of charge carriers. The same trend has also been observed for ZnO spin coated thin films by increasing the concentration of Sm^{3+} from 1 to 2 and 4 M percent [203] or by increasing the concentration of Ag^{2+} from 6 wt% to 10 wt% [201]. Thus, both doping element and its concentration should be considered to achieve high photocatalytic activity.

4.3. Spray coating/pyrolysis

Spray coating or spray pyrolysis is the term used for the atmospheric pressure chemical deposition of materials on a substrate by spraying the solution on a hot substrate where the pyrolysis reaction occurs [170, 205]. The coating layer is formed by the removal of all unstable materials at the working temperature [170]. This is a low cost method in which vacuum is not required [205]. Overall, spray pyrolysis is divided into three categories (based on the type of reaction) as follows [206]:

1. Residing the droplets of the solution on the heated substrate by evaporation of the solvent (further reaction of components could occur in the dry state),
2. Evaporation of the solvent prior to reaching the heated substrate and impingement of the dry solid on the substrate by decomposition, and
3. Evaporation of the solvent by approaching the droplets to the substrate followed by heterogeneous reaction of the solution components.

Various nanostructured products could be synthesized using spray pyrolysis. Therefore, it is known as a versatile synthetic process for the production of thin films and powders [207]. Schematic of spray pyrolysis apparatus used for the production of thin films is shown in Fig. 9(a).

Compared with common methods used for the deposition of thin

Table 6
Application of spin coating for deposition of photocatalytic TiO_2 and ZnO films.

Photocatalytic film	Thickness	Pollutant (concentration)	Source of light	Efficiency	Reference
Anatase TiO_2	38 ± 1	Acid yellow 17 (10 mg L^{-1})	UV	k = 0.13 μM h^{-1}	[204]
Anatase TiO_2	53 ± 1	Acid yellow 17 (10 mg L^{-1})	UV	k = 0.14 μM h^{-1}	[204]
Anatase TiO_2	63 ± 1	Acid yellow 17 (10 mg L^{-1})	UV	k = 0.42 μM h^{-1}	[204]
Anatase TiO_2	81 ± 1	Acid yellow 17 (10 mg L^{-1})	UV	k = 0.80 μM h^{-1}	[204]
Anatase TiO_2	93 ± 1	Acid yellow 17 (10 mg L^{-1})	UV	k = 1.07 μM h^{-1}	[204]
Anatase TiO_2	107 ± 1	Acid yellow 17 (10 mg L^{-1})	UV	k = 1.21 μM h^{-1}	[204]
Anatase TiO_2	121 ± 2	Acid yellow 17 (10 mg L^{-1})	UV	k = 1.32 μM h^{-1}	[204]
Anatase TiO_2	135 ± 2	Acid yellow 17 (10 mg L^{-1})	UV	k = 1.35 μM h^{-1}	[204]
Anatase TiO_2	149 ± 2	Acid yellow 17 (10 mg L^{-1})	UV	k = 1.40 μM h^{-1}	[204]
Anatase TiO_2	163 ± 2	Acid yellow 17 (10 mg L^{-1})	UV	k = 1.41 μM h^{-1}	[204]
TiO_2	NA	Rhodamine B (3 mM)	Sunlight	k = 1.25 $mmin^{-1}$	[198]
N-doped TiO_2 (3 wt%)	NA	Rhodamine B (3 mM)	Sunlight	k = 13.75 $mmin^{-1}$	[198]
N-doped TiO_2 (10 wt%)	NA	Rhodamine B (3 mM)	Sunlight	k = 7.50 $mmin^{-1}$	[198]
TiO_2	NA	Methylene blue (4 mg L^{-1})	UV	k = 0.018 h^{-1}	[199]
Fe^{3+}-doped TiO_2 (5 wt%)	NA	Methylene blue (4 mg L^{-1})	UV	k = 0.023 h^{-1}	[199]
Fe^{3+}-doped TiO_2 (10 wt%)	NA	Methylene blue (4 mg L^{-1})	UV	k = 0.024 h^{-1}	[199]
Fe^{3+}-doped TiO_2 (15 wt%)	NA	Methylene blue (4 mg L^{-1})	UV	k = 0.028 h^{-1}	[199]
Fe^{3+}-doped TiO_2 (20 wt%)	NA	Methylene blue (4 mg L^{-1})	UV	k = 0.036 h^{-1}	[199]
Fe^{3+}-doped TiO_2 (25 wt%)	NA	Methylene blue (4 mg L^{-1})	UV	k = 0.038 h^{-1}	[199]
ZnO	367.7 nm	Methylene blue (1×10^{-5} M)	UV	89.3 % (t = 7 h)**	[203]
Sm^{3+}-doped ZnO (1 mol%)	354.5 nm	Methylene blue (1×10^{-5} M)	UV	90.4 % (t = 7 h)**	[203]
Sm^{3+}-doped ZnO (2 mol%)	360.7 nm	Methylene blue (1×10^{-5} M)	UV	88.1 % (t = 7 h)**	[203]
Sm^{3+}-doped ZnO (4 mol%)	361.3 nm	Methylene blue (1×10^{-5} M)	UV	68.2 % (t = 7 h)**	[203]
ZnO	NA	Methylene blue (1×10^{-5} M)	Visible	k = 0.00547 min^{-1}	[200]
Co-doped ZnO (5 wt%)	NA	Methylene blue (1×10^{-5} M)	Visible	k = 0.00688 min^{-1}	[200]
Co-doped ZnO (10 wt%)	NA	Methylene blue (1×10^{-5} M)	Visible	k = 0.00932 min^{-1}	[200]
Co-doped ZnO (15 wt%)	NA	Methylene blue (1×10^{-5} M)	Visible	k = 0.01340 min^{-1}	[200]
ZnO	NA	Reactive Red 195 (10 mg L^{-1})	Simulated solar light	k: ~0.0021 min^{-1}	[201]
Ag-doped ZnO (2 wt%)	NA	Reactive Red 195 (10 mg L^{-1})	Simulated solar light	k: ~0.0021 min^{-1}	[201]
Ag-doped ZnO (4 wt%)	NA	Reactive Red 195 (10 mg L^{-1})	Simulated solar light	k: ~0.0028 min^{-1}	[201]
Ag-doped ZnO (6 wt%)	NA	Reactive Red 195 (10 mg L^{-1})	Simulated solar light	k: ~0.0037 min^{-1}	[201]
Ag-doped ZnO (8 wt%)	NA	Reactive Red 195 (10 mg L^{-1})	Simulated solar light	k: ~0.0025 min^{-1}	[201]
Ag-doped ZnO (10 wt%)	NA	Reactive Red 195 (10 mg L^{-1})	Simulated solar light	k: ~0.0014 min^{-1}	[201]
Ag-doped ZnO (6 wt%)	NA	Reactive Red 195 (15 mg L^{-1})	Simulated solar light	k: ~0.0016 min^{-1}	[201]
Ag-doped ZnO (6 wt%)	NA	Reactive Red 195 (20 mg L^{-1})	Simulated solar light	k: ~0.0007 min^{-1}	[201]
Ag-doped ZnO (6 wt%)	NA	Reactive Red 195 (25 mg L^{-1})	Simulated solar light	k: ~0.0006 min^{-1}	[201]
ZnO	NA	Reactive Yellow 145 (10 mg L^{-1})	Simulated solar light	k: ~0.0016 min^{-1}	[201]
Ag-doped ZnO (2 wt%)	NA	Reactive Yellow 145 (10 mg L^{-1})	Simulated solar light	k: ~0.0018 min^{-1}	[201]
Ag-doped ZnO (4 wt%)	NA	Reactive Yellow 145 (10 mg L^{-1})	Simulated solar light	k: ~0.0030 min^{-1}	[201]
Ag-doped ZnO (6 wt%)	NA	Reactive Yellow 145 (10 mg L^{-1})	Simulated solar light	k: ~0.0040 min^{-1}	[201]
Ag-doped ZnO (8 wt%)	NA	Reactive Yellow 145 (10 mg L^{-1})	Simulated solar light	k: ~0.0026 min^{-1}	[201]
Ag-doped ZnO (10 wt%)	NA	Reactive Yellow 145 (10 mg L^{-1})	Simulated solar light	k: ~0.0018 min^{-1}	[201]
Ag-doped ZnO (6 wt%)	NA	Reactive Yellow 145 (15 mg L^{-1})	Simulated solar light	k: ~0.0022 min^{-1}	[201]
Ag-doped ZnO (6 wt%)	NA	Reactive Yellow 145 (20 mg L^{-1})	Simulated solar light	k: ~0.0016 min^{-1}	[201]
Ag-doped ZnO (6 wt%)	NA	Reactive Yellow 145 (25 mg L^{-1})	Simulated solar light	k: ~0.0011 min^{-1}	[201]
ZnO	NA	Reactive Orange 122 (10 mg L^{-1})	Simulated solar light	k: ~0.0018 min^{-1}	[201]
Ag-doped ZnO (2 wt%)	NA	Reactive Orange 122 (10 mg L^{-1})	Simulated solar light	k: ~0.0025 min^{-1}	[201]
Ag-doped ZnO (4 wt%)	NA	Reactive Orange 122 (10 mg L^{-1})	Simulated solar light	k: ~0.0037 min^{-1}	[201]
Ag-doped ZnO (6 wt%)	NA	Reactive Orange 122 (10 mg L^{-1})	Simulated solar light	k: ~0.0054 min^{-1}	[201]
Ag-doped ZnO (8 wt%)	NA	Reactive Orange 122 (10 mg L^{-1})	Simulated solar light	k: ~0.0037 min^{-1}	[201]
Ag-doped ZnO (10 wt%)	NA	Reactive Orange 122 (10 mg L^{-1})	Simulated solar light	k: ~0.0030 min^{-1}	[201]
Ag-doped ZnO (6 wt%)	NA	Reactive Orange 122 (15 mg L^{-1})	Simulated solar light	k: ~0.0034 min^{-1}	[201]
Ag-doped ZnO (6 wt%)	NA	Reactive Orange 122 (20 mg L^{-1})	Simulated solar light	k: ~0.0024 min^{-1}	[201]
Ag-doped ZnO (6 wt%)	NA	Reactive Orange 122 (25 mg L^{-1})	Simulated solar light	k: ~0.0020 min^{-1}	[201]

Note: ** (Contribution of degradation).

films, spray pyrolysis can take advantages of specific properties. General advantages and limitations of spray pyrolysis are provided in Table 7.

In general, this technique involves separate individual stages that includes atomization, transport of aerosol, and precursor decomposition [207]. Thus, selection of the solvent, type of precursor, aerosol droplet size distribution, synthesis temperature, nature of carrier gas and its flux rate could affect the morphology of deposited materials [205]. The main parameters that can be easily controlled consists nozzle to substrate distance, synthesis temperature, concentration of the precursor solution, and the flux rate of carrier gas [206]. Owing to the strong dependency of the droplets drying, grain growth, decomposition, and crystallization on temperature, the substrate temperature is known as the most important parameter among these factors [170,206]. The more the substrate temperature, the higher are the roughness and the porosity of the deposited films, whereas using too low temperatures could result in the formation of cracks in the thin film. Notably, the deposition temperature could affect the crystallinity, texture, and phase composition of the films deposited by spray pyrolysis [207]. Overall, four different processes could occur by an increase in the substrate temperature as shown in Fig. 9(b). In process A (at the lowest temperature regime), the droplets hit the surface and decompose. In process B (at higher temperatures), evaporation of the solvent occurs during the flight of droplets. Thus, dry precipitate hits the surface of the substrate. In process C (at higher temperatures), although evaporation of the solvent occurs prior to hitting the droplets to the substrate, melting and evaporation of the dry precipitate is observed (without decomposition). Afterward, diffusion of vapor to the substrate takes place to perform a CVD process. In process D (at the highest temperatures), evaporation of the precursor occurs prior to reaching the substrate [209]. The solid particles will be formed in the vapor phase by the chemical reactions, consequently. In general, it has

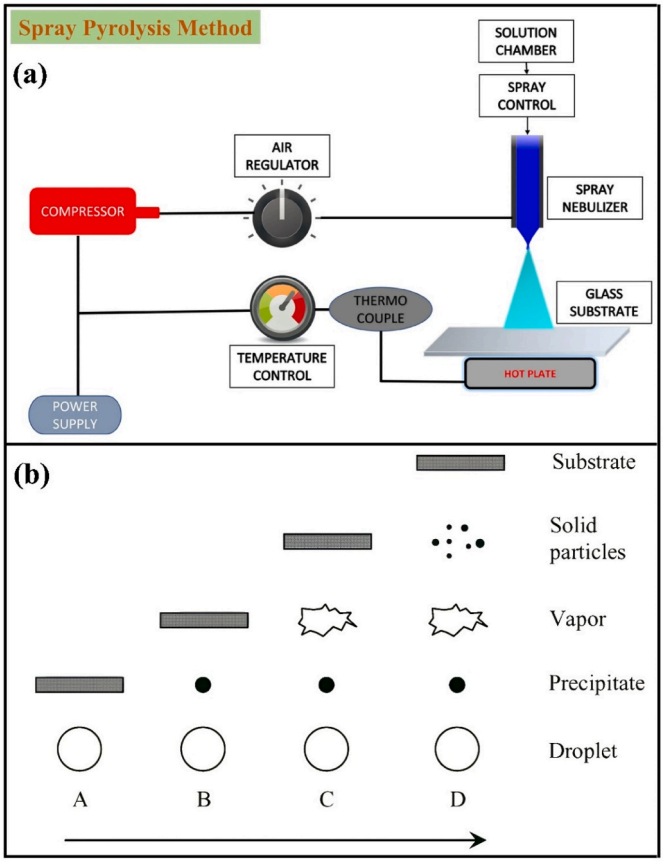

Fig. 9. (a) Schematic of spray pyrolysis apparatus used to produce thin films. Reproduced with permission from Ref. [208] Copyright 2023 Springer Nature. The rights of this figure are owned by a third party. (b) Description of the deposition processes accompanied by increase of the substrate temperature. Reproduced with permission from Ref. [209] Copyright 2005 Springer Nature. The rights of this figure are owned by a third party.

been stated that non-adherent (and/or rough) films are generated in processes A and D. It is while, adherent films could be formed in process C. Notably, processes A and B could also lead to the preparation of high quality adherent films [209]. Khoury et al. [85] deposited ZnO using various methods including reactive electron-beam evaporation, RF magnetron sputtering, and electrostatic spray pyrolysis. Although PVD (both electron-beam evaporation and reactive RF magnetron sputtering) resulted in the formation of c-axis oriented ZnO film, electrostatic spray pyrolysis fabricated polycrystalline ZnO film with a (002) preferred orientation. Notably, ZnO film deposited by electron-beam evaporation showed the best crystallinity between these three methods. Although the nature of the residual stress was different in the fabricated films, those deposited by electrostatic spray pyrolysis (compressive stress) and reactive electron-beam evaporation (tensile stress) showed lower stress than that deposited by reactive RF magnetron sputtering (compressive stress). Noteworthy, the maximum transmittance, in the visible light region, was attributed to ZnO film deposited by reactive RF magnetron sputtering, electrostatic spray pyrolysis, and reactive electron-beam evaporation, respectively. It is notable that ZnO film deposited by reactive electron-beam evaporation showed smaller band gap energy than those deposited by electrostatic spray pyrolysis and reactive RF magnetron sputtering which has been attributed to its residual tensile stress (unlike ZnO films deposited by reactive RF magnetron sputtering and electrostatic spray pyrolysis with residual compressive stresses). Although Khoury et al. [85] suggested that residual compressive stresses could increase the band gap energy [85], a reciprocal behavior has been observed by Ghazzal et al. [182] where three different substrates were used to deposit TiO_2 thin films by sol-gel. Negligible, medium, and large residual compressive stresses were developed using soda-lime glass, borosilicate glass, and quartz substrate, respectively. Notably, the red-shift absorbance edge of TiO_2 deposited on borosilicate glass and quartz substrates has been directly attributed to the increased residual compressive stress [182]. All in all, residual stress (tensile or compressive) could affect the band gap energy of materials, their band's shape, and optical properties [210–212]. It is worth mentioning that the residual tensile stress could induce fatigue crack initiation and environmentally-assisted cracking in the deposited films [213], whereas the residual compressive stress could lead to the film debonding and buckling (formation of open channels) [214]. Compared with electron-beam evaporation and magnetron sputtering techniques, spray pyrolysis could suffer from the fabrication of non-quite homogeneous films as illustrated in Fig. 10 [85].

The same as spin coating, deposition of photocatalytic TiO_2 and ZnO films using spray coating has been widely studied some of which are provided in Table 8. As evident, nitrogen doping (up to 2 at%) considerably increased the photocatalytic activity of TiO_2 thin films deposited by spray pyrolysis. However, further increase of nitrogen doping, up to 4 at% and 6 at%, decreased the photocatalytic degradation of methylene blue [215]. The same trend has also been observed for Er-doped ZnO thin films. Although an increase in the concentration of Er (up to 1.0 at

Table 7
General advantages and limitations of spray pyrolysis.

Advantages [170,205,207,209]
a) Low cost
b) No need for vacuum
c) Deposition of various metal oxides and compounds
d) Formation of mixed and/or multiple layered structures
e) Easy adaptation for large area production
f) Use of highly diluted solutions
g) Deposition of dense and porous films
h) Deposition of doped metal oxides
i) Easy control of the components and morphology of the target material
j) No requirement for the substrate preparation
k) Possibility of deposition on non-flat areas using a hand-held sprayer
l) Possibility of deposition over a wide variety of substrates
m) No need to high quality substrates or chemicals
Disadvantages [205–207]
a) Wide variety of parameters affecting the quality of deposited film
b) Difficulty of controlling the parameters during the process
c) Inherently non-uniform thickness of the deposited films
d) High dependency of the properties of deposited films on substrate properties
e) Imposing remarkable heat tolerance requirements for the substrate

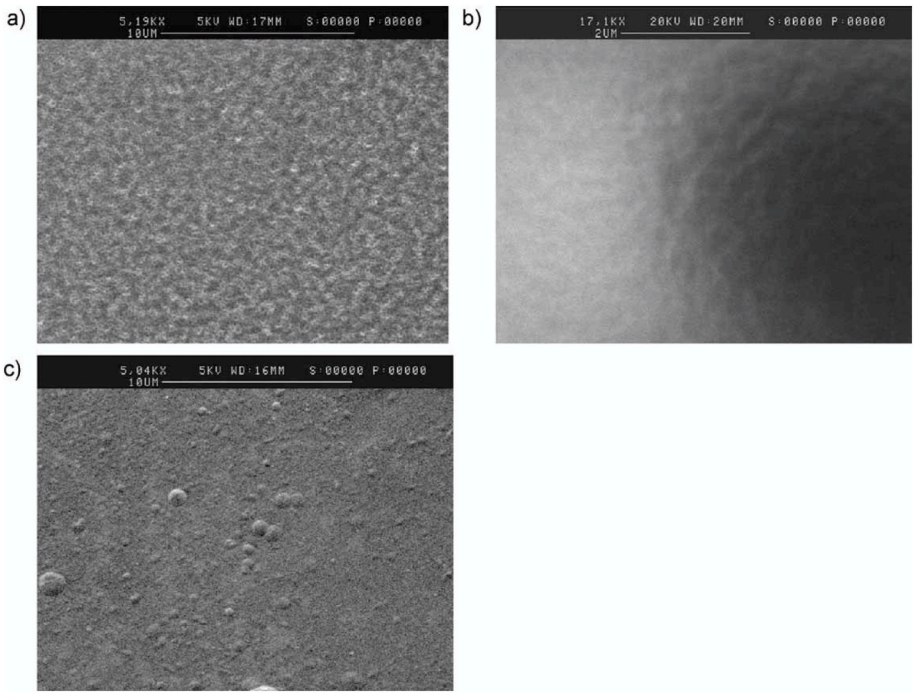

Fig. 10. SEM micrographs of ZnO thin films on Si (100) deposited by (a) electron-beam evaporation, (b) RF magnetron sputtering, and (c) electrostatic spray pyrolysis. Reproduced with permission from Ref. [85] Copyright 2010 John Wiley and Sons.

Table 8
Application of spray coating in deposition of photocatalytic TiO_2 and ZnO films.

Photocatalytic film	Thickness	Pollutant (concentration)	Source of light	Efficiency	Reference
TiO_2	NA	Methylene blue (2 mg L^{-1})	UV	63.3 % (t = 3 h)	[215]
N-doped TiO_2 (2 at%)	NA	Methylene blue (2 mg L^{-1})	UV	94 % (t = 3 h)	[215]
N-doped TiO_2 (4 at%)	NA	Methylene blue (2 mg L^{-1})	UV	~86 % (t = 3 h)	[215]
N-doped TiO_2 (6 at%)	NA	Methylene blue (2 mg L^{-1})	UV	~70 % (t = 3 h)	[215]
ZnO	254 nm	Methylene blue (2.5×10^{-5} M)	UV	k = 1.45 h^{-1}	[217]
ZnO nanoflakes	370 ± 7 nm	Methyl orange (1×10^{-5} M)	UV	k = 0.0121 min^{-1}	[218]
ZnO nanorods	480 ± 107 nm	Methyl orange (1×10^{-5} M)	UV	k = 0.0079 min^{-1}	[218]
ZnO	NA	Methylene blue (10 mg L^{-1})	UV	k = 0.00679 min^{-1}	[219]
Ag-doped ZnO (5 mol%)	NA	Methylene blue (10 mg L^{-1})	UV	k = 0.00638 min^{-1}	[219]
Ag-doped ZnO (10 mol%)	NA	Methylene blue (10 mg L^{-1})	UV	k = 0.00678 min^{-1}	[219]
Ag-doped ZnO (15 mol%)	NA	Methylene blue (10 mg L^{-1})	UV	k = 0.00802 min^{-1}	[219]
Ag-doped ZnO (20 mol%)	NA	Methylene blue (10 mg L^{-1})	UV	k = 0.00714 min^{-1}	[219]
Ag-doped ZnO (25 mol%)	NA	Methylene blue (10 mg L^{-1})	UV	k = 0.00969 min^{-1}	[219]
ZnO	397 nm	Rhodamine B (0.1 mg L^{-1})	UV	k = 0.026 min^{-1}	[216]
Er-doped ZnO (0.5 at%)	439 nm	Rhodamine B (0.1 mg L^{-1})	UV	k = 0.032 min^{-1}	[216]
Er-doped ZnO (1.0 at%)	453 nm	Rhodamine B (0.1 mg L^{-1})	UV	k = 0.038 min^{-1}	[216]
Er-doped ZnO (1.5 at%)	441 nm	Rhodamine B (0.1 mg L^{-1})	UV	k = 0.035 min^{-1}	[216]
N-doped ZnO-CuO nanocomposite	NA	Methyl orange (20 mg L^{-1})	UV	~80 % (t = 75 min)	[220]
Fe-doped ZnO (5 %)	NA	Rhodamine B (10 mg L^{-1})	Visible	64.53 % (t = 3 h)	[221]
Fe-doped ZnO (10 %)	NA	Rhodamine B (10 mg L^{-1})	Visible	65.57 % (t = 3 h)	[221]
Fe-doped ZnO (15 %)	NA	Rhodamine B (10 mg L^{-1})	Visible	67.36 % (t = 3 h)	[221]
Fe-doped ZnO (20 %)	NA	Rhodamine B (10 mg L^{-1})	Visible	70.79 % (t = 3 h)	[221]
Fe-doped ZnO (5 %)	NA	Methylene blue (10 mg L^{-1})	Visible	60.64 % (t = 3 h)	[221]
Fe-doped ZnO (10 %)	NA	Methylene blue (10 mg L^{-1})	Visible	62.53 % (t = 3 h)	[221]
Fe-doped ZnO (15 %)	NA	Methylene blue (10 mg L^{-1})	Visible	62.34 % (t = 3 h)	[221]
Fe-doped ZnO (20 %)	NA	Methylene blue (10 mg L^{-1})	Visible	65.31 % (t = 3 h)	[221]

%), improved the photocatalytic activity, further increase of Er deteriorated the photocatalytic efficiency [216].

5. Deposition of thick/thin films using solid particles

There are different methods that can be used for deposition of solid particles. Electrophoretic deposition and thermal spraying are among the main methods which can be effectively used for the fabrication of thick/thin and dense coatings (using solid particles). Notably, the application of thermal spraying processes in the production of TiO_2 and ZnO films was studied in our previous research [26]. Hence, the application of EPD in deposition of TiO_2 and ZnO is studied in this research.

5.1. Electrophoretic deposition

EPD is an electrochemical method for processing both coating and bulk materials. Although it has been discovered in the early 1800s, it has received remarkable attention to produce advanced materials as a promising technology in both industry and academia [222]. Due to its compatibility with a variety of materials, EPD has been receiving

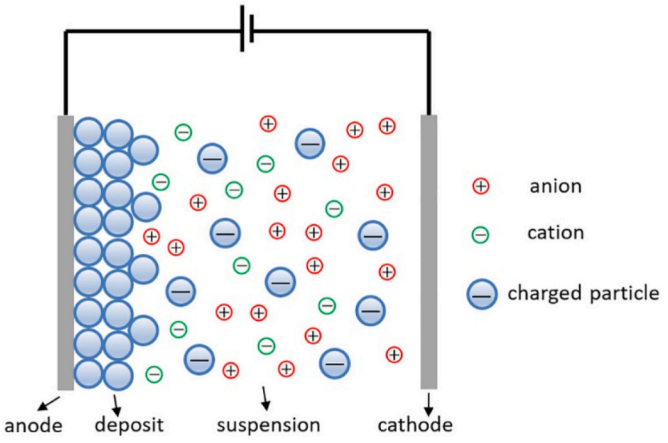

Fig. 11. Schematic illustration of electrophoretic deposition. Reproduced with permission from Ref. [227] Copyright 2020 Elsevier.

growing attention as a manufacturing process [223]. However, it is mainly used for deposition of ceramic materials [222]. EPD is a two-step process where the suspended particles (in colloidal solutions) are collected on a substrate. Deposition process occurs in an electrochemical cell where the substrate material is used as one of the electrodes. Polarization of the suspended particles by an appropriate applied potential (using a direct current electric field), pulls them toward the oppositely charged electrode (substrate). It leads to the formation of a relatively compact and homogeneous coating, consequently [149,224]. However, the resulted film is just a powder agglomeration at this stage. Further processing, such as sintering/heat treatment, is needed to improve the bonds between the substrate and agglomerated particles [224] or to ensure crystallinity [225]. An appropriate suspension for electrophoretic deposition should have several features including high particle surface charge (to improve the ceramic particle mobility), low viscosity (to improve the ceramic particle mobility), high dielectric constant of liquid phase, and low conduction of the suspending medium (to decrease the transport of solvent) [226]. Thickness and morphology of the deposited films rely on deposition time and strength of electric field [149,225]. Overall, EPD can be used for deposition of any solid particle in the form of colloidal suspension or fine powder (particle size $< \sim 30$ μm). Besides, this process can be used for deposition of functionally graded ceramic coatings with a wide range of thickness from less than 1 μm to more than 500 μm. Moreover, this process is capable of using complex-shaped substrates [149]. Schematic illustration of EPD is shown in Fig. 11, and its major merits and drawbacks are presented in Table 9.

Electrophoretic deposition has received remarkable attention for the fabrication of photocatalytic TiO_2 coatings some of which are provided in Table 10. Although electrophoretic deposition of TiO_2 takes advantages of its low temperature (during deposition), further annealing/calcination at high temperatures is generally needed to improve the quality/adhesion of coatings or remove organic compounds [233–238]. For example, Singh et al. [238] deposited TiO_2 nanoparticles, synthesized by microwave method, using EPD at room temperature, whereas the deposited film was annealed at 500 °C for 2 h. Notably, the deposited TiO_2 film showed higher efficiency than initially-synthesized TiO_2 nanoparticles for the photocatalytic degradation of methyl red. Mahammadi et al. [233] evaluated the effects of some key parameters in electrophoretic deposition (including deposition time, calcination temperature, applied voltage, and weight percentage of photocatalyst) on the photocatalytic activity of nanocrystalline titania films (using P25 nanoparticles). Between the applied voltages of 10 V, 30 V, and 50 V, TiO_2 film deposited at 30 V showed the highest photocatalytic activity. Notably, the formation of numerous cracks inhibited the production of uniform films at 10 V and 50 V. Increasing the calcination temperature from 300 °C to 500 °C and 700 °C suppressed the photocatalytic activity which has been attributed to the increase of rutile phase content (or decrease of anatase phase content) and acceleration of the growth of crystallites. Increasing the deposition time from 1 min to 3 min and 5 min enhanced the photocatalytic efficiency, clarifying the effect of thickness on the photocatalytic activity of TiO_2 coatings. Increasing the weight percentage of P25 from 0.2 wt% to 0.6 wt% and 1 wt% also improved the photocatalytic activity. It has been shown that the initial concentration of suspended TiO_2 nanoparticles could significantly affect the structural and morphological properties of titania films, where using the weight percentage of 1 wt% resulted in the formation of smoother, more uniform, and more dense titania films (with less cracks) with a higher photocatalytic activity. Analysis of variance (ANOVA) analysis introduced applied voltage and P25 wt percentage as the least and the most influential parameters, respectively, on the photocatalytic activity in their research.

Hosseini et al. [235] used EPD for the fabrication of pure TiO_2 and TiO_2/Ag thin films (with the thickness of a few hundred nanometers) on stainless steel substrates for the photocatalytic degradation of methylene blue. Although TiO_2/Ag thin films showed higher photocatalytic activity than pure TiO_2 thin films (due to the more efficient separation of photogenerated e^-/h^+ pairs), variation of either deposition time (from 0.5 min to 5 min) or current density (from 400 μA cm^{-2} to 2000 μA cm^{-2}) did not significantly affect the photocatalytic activity in both cases. In another research, Teodoro et al. [236] synthesized Cu-doped TiO_2

Table 9
General merits and drawbacks of EPD.

Advantages [149,228–232]
a) None line of sight coating process
b) High deposition rate
c) Low cost
d) Simple apparatus
e) High purity of deposited films
f) High microstructural homogeneity of deposited films
g) No requirement to additives or binders
h) Deposition of uniform films
i) Capability of depositing porous microstructures
j) Capability of using complex-shaped substrates
k) Capability of using substrates with large surface area
l) Control of the coating thickness, from thin films to thick films, and structure of the coatings
Disadvantages [149,229,232]
a) Using an appropriate solvent for suspension stabilization and provision of high electrophoretic mobility
b) Poor adhesion
c) Possible generation of cracks at the interface of coating/substrate or on the surface of film
d) Limitation of using conductive substrates
e) High costs of preparing large components

Table 10
Application of EPD in the fabrication of photocatalytic TiO_2 films.

Photocatalytic film	Thickness	Pollutant (concentration)	Source of light	Efficiency	Reference
TiO_2	NA	Methyl orange (5 mg L^{-1})	UV	83 % on average (t = 3 h)	[233]
TiO_2	NA	4-chlorophenol (NA)	UV	61 % (t = 5 h)**	[239]
TiO_2-rGO (0.5 wt%)	NA	4-chlorophenol (NA)	UV	84 % (t = 5 h)**	[239]
TiO_2	NA	Methylene blue (10 mg L^{-1})	UV	35 % (t = 5 h)	[240]
TiO_2	NA	Methylene blue (10 mg L^{-1})	Visible	26 % (t = 5 h)	[240]
TiO_2	NA	Methylene blue (10 mg L^{-1})	Sunlight	62 % (t = 5 h)	[240]
AgCl-TiO_2	162.9 nm	Methamphetamine (20 mg L^{-1})	Natural solar light	25 % (t = 2 h)	[241]
AgCl-TiO_2	325.7 nm	Methamphetamine (20 mg L^{-1})	Natural solar light	49 % (t = 2 h)	[241]
AgCl-TiO_2	651.5 nm	Methamphetamine (20 mg L^{-1})	Natural solar light	68 % (t = 2 h)	[241]
AgCl-TiO_2	977.2 nm	Methamphetamine (20 mg L^{-1})	Natural solar light	84 % (t = 2 h)	[241]
AgCl-TiO_2	1302.9 nm	Methamphetamine (20 mg L^{-1})	Natural solar light	94 % (t = 2 h)	[241]
AgCl-TiO_2	1628.7 nm	Methamphetamine (20 mg L^{-1})	Natural solar light	95 % (t = 2 h)	[241]
AgCl-TiO_2	1954.4 nm	Methamphetamine (20 mg L^{-1})	Natural solar light	95 % (t = 2 h)	[241]
Sn-doped TiO_2	NA	Methylene blue (10 mg L^{-1})	UV	51 % (t = 5 h)	[240]
Sn-doped TiO_2	NA	Methylene blue (10 mg L^{-1})	Visible	47 % (t = 5 h)	[240]
Sn-doped TiO_2	NA	Methylene blue (10 mg L^{-1})	Sunlight	73 % (t = 5 h)	[240]
Cu-doped TiO_2 (0.5 at%)	~125 μm	Rhodamine B (1×10^{-5} M)	UV	56.3 % (t = 1 h)**	[236]
0.5N-doped TiO_2	–	Methylene blue (NA)	Visible	k = 0.1807 h^{-1}	[237]
0.1Fe-0.5N-doped TiO_2	–	Methylene blue (NA)	Visible	k = 0.184 h^{-1}	[237]
TiO_2	5.3 μm	Amido black-10B (10 mg L^{-1})	UV	80.97 % (t = 5 h)**	[242]
TiO_2-WO_3 (1 wt%)	8.4 μm	Amido black-10B (10 mg L^{-1})	UV	81.31 % (t = 5 h)**	[242]
TiO_2-WO_3 (2 wt%)	9.5 μm	Amido black-10B (10 mg L^{-1})	UV	82.86 % (t = 5 h)**	[242]
TiO_2-WO_3 (3 wt%)	11.5 μm	Amido black-10B (10 mg L^{-1})	UV	84.21 % (t = 5 h)**	[242]
TiO_2-WO_3 (4 wt%)	12.7 μm	Amido black-10B (10 mg L^{-1})	UV	86.88 % (t = 5 h)**	[242]
TiO_2-WO_3 (5 wt%)	21 μm	Amido black-10B (10 mg L^{-1})	UV	88.34 % (t = 5 h)**	[242]

Note: ** (Contribution of degradation).

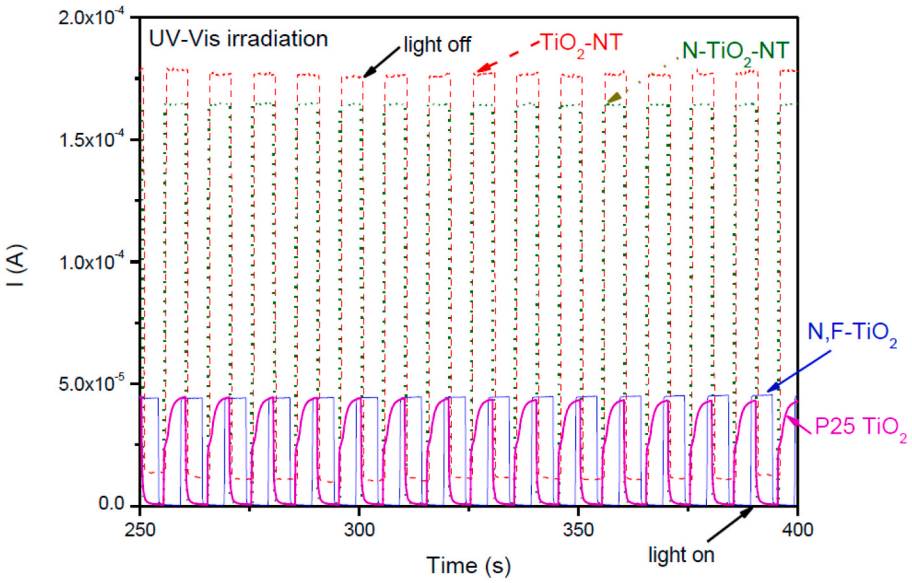

Fig. 12. Photocurrents of electrodes obtained by TiO_2 nanotubes (fabricated by anodizing), N-doped TiO_2 nanotubes (fabricated by anodizing), P25 TiO_2 nanoparticles (deposited by EPD), and N,F-doped TiO_2 nanoparticles (deposited by EPD) in ¼ strength solution under chopped UV–vis illumination (potential bias = 1 V and UV–vis exposure time = 5 s). 3rd cycle of current measurement for each electrode. Reproduced with permission from Ref. [234] Copyright 2017 MDPI. This article is an open access article distributed under the terms and conditions of the Creative Commons Attribution (CC BY) license (http://creativecommons.org/licenses/by/4.0/).

particles. Notably, it has been shown that Cu doping up to 0.5 at% could promote the stability of anatase phase and reduce the band gap energy. Then, Cu-doped TiO_2 particles were deposited by EPD on an aluminum substrate for the degradation of Rhodamine B, where pure TiO_2 and Cu-doped TiO_2 particles provided higher degradation rates than the deposited film (63.9 %, 98.3 %, and 56.3 % within 1 h, respectively). The possibility of depositing rough and porous surfaces, as observed by Teodoro et al. [236], could introduce EPD as a substantial alternative to those methods that can fabricate flat surfaces. Pablos et al. [234] fabricated TiO_2 thin films by different methods of anodizing (using Ti substrate) and electrophoretic deposition (using TiO_2 nanoparticles). The photocurrents of TiO_2 nanotubes (fabricated by anodizing) and TiO_2 nanoparticles (deposited by EPD) are compared in Fig. 12.

As shown, nanotubular structures provided higher photocurrent than nanoparticles. Compared with nanoparticles, aligned nanotubular structures could yield a more direct pathway for the transfer of electrons, resulting in the higher photocurrent of TiO_2 films fabricated by anodizing. On the downside, nanotubular structures generally suffer from their lower specific surface area than mesoporous nanoparticle thick films [234] which could be fabricated by some methods e.g. EPD. Zlamal et al. [243] fabricated both nanotubular and P25 (nanoparticles) TiO_2 electrodes for electrochemically assisted photocatalysis. The

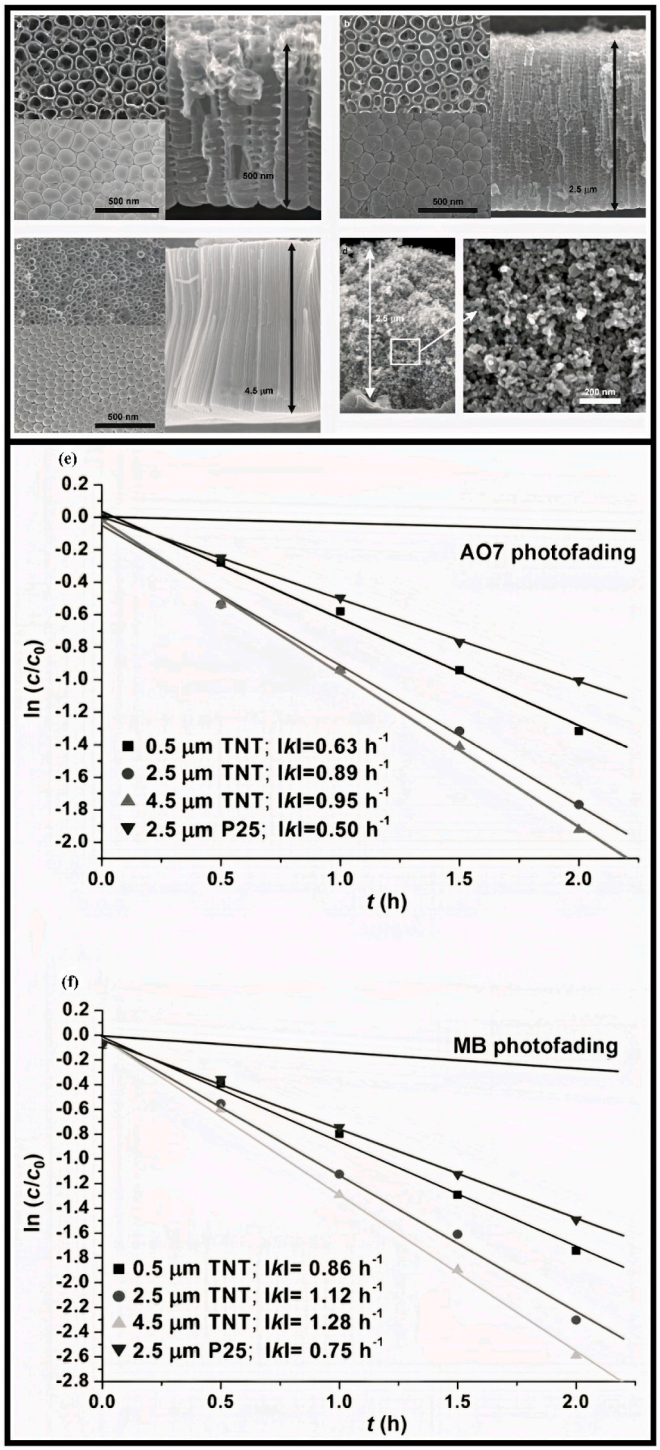

Fig. 13. (a–c) SEM micrographs of anodic titania nanotubular films with different thicknesses of 0.5 μm, 2.5 μm, and 4.5 μm. (d) SEM micrograph of thick Degussa P25 film (2.5 μm). (e) Photocatalysis of AO7. (f) Photocatalysis of methylene blue. Reproduced with permission from Ref. [244] Copyright 2007 John Wiley and Sons.

specific surface area of the thick titania nanotubular structure with the thickness of 2.5 μm, i.e. 12 m^2 g^{-1}, was considerably lower than that of P25 electrode, i.e. 50 m^2 g^{-1}, signifying the crucial importance of nanoparticles deposition. However, the electronic properties of TiO_2 nanotubular morphology was superior than that of P25 nanoparticles. The same trend has also been reported by Macak et al. [244], where nanotubular and P25 (nanoparticles) TiO_2 films were fabricated for the

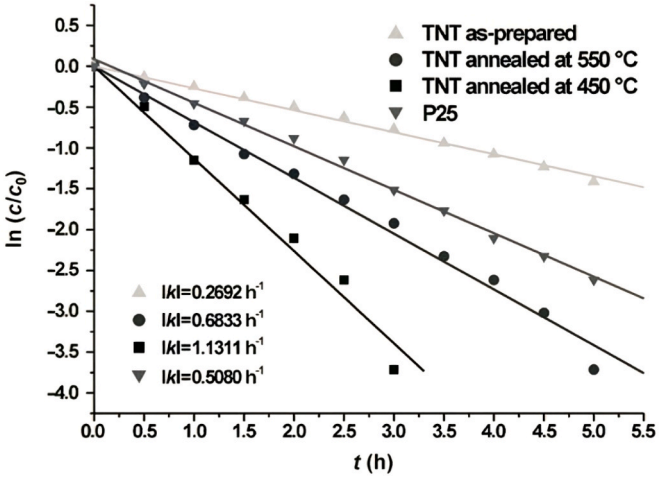

Fig. 14. Comparison of the photocatalytic degradation rates of AO7 using as-prepared TiO_2 nanotubes, TiO_2 nanotubes annealed at 450 °C, TiO_2 nanotubes annealed at 550 °C, and P25 film (with the similar thicknesses of 2.5 μm). Reproduced with permission from Ref. [244] Copyright 2007 John Wiley and Sons.

photocatalytic degradation of Acid orange 7 (AO7) and methylene blue. SEM micrographs and the photocatalytic degradation rates of AO7 and methylene blue by using TiO_2 nanotube films, with the thicknesses of 0.5 μm, 2.5 μm, and 4.5 μm, and by using P25 TiO_2 film, with the thickness of 2.5 μm, are shown in Fig. 13.

As evident, increasing thickness improved the photocatalytic activity of TiO_2 nanotubes, and all nanotubular films showed higher photocatalytic activity than Degussa P25 film for both AO7 and methylene blue. It is while nanotubular films had significantly smaller active surface than P25 film (approximately 7 times). Notably, the nanotubular morphology could provide an optimized geometry to shorten the carrier-diffusion paths and lower the recombination rate of charge carriers [244]. However, it should be noted that the crystal structure of the nanotubular TiO_2 films fabricated by Macak et al. [244] were different from P25 nanoparticles with 80 wt% of anatase and 20 wt% of rutile phases. Due to the amorphous structure of the as-prepared samples by anodizing, they were annealed at 450 °C and 550 °C to fabricate pure anatase and mixture of anatase/rutile phases, respectively. It is while the crystal structure (ratio of anatase to rutile) can significantly affect the photocatalytic performance e.g. the appearance of small traces of rutile phase in the sample annealed at 550 °C remarkably decreased the photocatalytic degradation rate of AO7 from 1.1311 h^{-1} to 0.6833 h^{-1} compared with the sample annealed at 450 °C (with pure anatase phase). Thus, the fewer anatase phase content of P25 should have played an important role in the lower photocatalytic activity of P25 film than nanotubular TiO_2 films. Photocatalytic degradation rates of AO7 using the as-prepared TiO_2 nanotubes, the nanotubes annealed at 450 °C, the nanotubes annealed at 550 °C, and the P25 film (with the similar thicknesses of 2.5 μm) are compared in Fig. 14, signifying the effect of the crystal structure on the photocatalytic activity of TiO_2 films.

In addition to TiO_2, there are some studies on electrophoretic deposition of ZnO particles in which the effects of process parameters on the quality of ZnO films have been evaluated [245–247]. Wang et al. [246] introduced EPD as a powerful method for the fabrication of uniform nanostructured ZnO coatings with desired thickness and excellent smoothness by using narrow size distribution and small particle size (ZnO nanoparticles). Similar to TiO_2 coatings [233,235], it has been shown that deposition time and applied voltage could affect the properties of ZnO films fabricated by EPD, where increasing deposition time and applied voltage increased the thickness of ZnO films. Besides, it has been shown that the uniformity of films is affected by the particle size of the initial ZnO powder used in EPD, where using smaller particle size

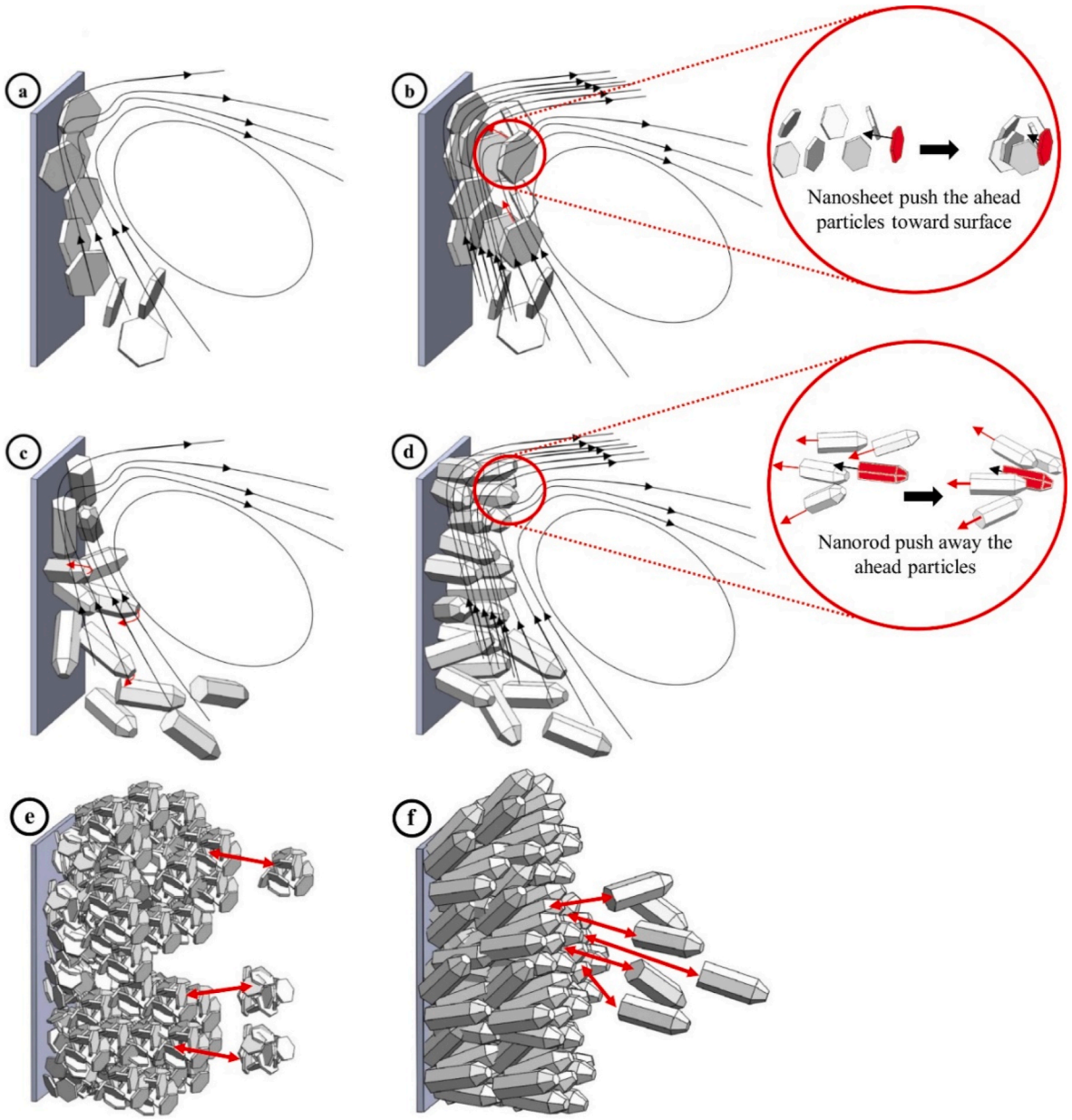

Fig. 15. Schematic illustration of the attachment of ZnO nanorods and ZnO nanosheets at different voltages: (a) ZnO nanosheets at low voltages, (b) ZnO nanosheets at high voltages, (c) ZnO nanorods at low voltages, (d) ZnO nanorods at high voltages. Formation of films at high voltages using (e) ZnO nanosheets and (f) ZnO nanorods. Reproduced with permission from Ref. [245] Copyright 2018 Elsevier.

and more stable suspension could lead to the higher uniformity of coatings (because of better packing) [246]. Similar to TiO_2 films, as-deposited ZnO films produced by EPD need a post-heat treatment for improvement of their quality. Notably, porosity of the deposited films could be easily controlled by the annealing temperature e.g. Jun et al. fabricated pore-free ZnO films by sintering the as-deposited films at 850 °C and 1050 °C for 2 h [247]. Mohammadi et al. [245] used the EPD process for the fabrication of two different morphologies of ZnO (i.e. ZnO nanorods with the average diameter of 139 nm and ZnO nanosheets with the average thickness of 26 nm). Under similar conditions of deposition, ZnO nanosheets showed a higher deposition rate than ZnO nanorods. Besides, compared with ZnO nanorods, ZnO nanosheets resulted in the fabrication of denser films. However, ZnO nanorods provided more uniform coatings at different voltages. Schematic illustration of the attachment of ZnO nanorods and ZnO nanosheets (at low and high voltages) and the formation of films at high voltages are compared in Fig. 15.

It has been shown that applied voltage could significantly affect the morphology of ZnO films. Notably, flower-like structures were fabricated using ZnO nanorods at high voltages which has been attributed to the sudden attachment of nanorods to the substrate and the formation of packed ZnO nanoparticles followed by the prevention of other nanoparticles to lie down adjacent to the former nanoparticles. Compared with ZnO nanorods, ZnO nanosheets provided coatings with higher porosity at high voltages [245]. Overall, it can be concluded that the morphology of initial particles could remarkably affect the quality of TiO_2/ZnO films fabricated by EPD. Noteworthy, EPD can be used for deposition of ZnO/TiO_2 coatings with high porosity and high surface area that are desired for photocatalytic applications. To exemplify, Taheri et al. [248] used a combination of sol-gel and EPD processes for deposition of nanostructured ZnO coatings with urchin-like morphologies, where a colloidal sol containing zinc acetate, trimethylamine, and methanol were used for deposition of urchin-like ZnO films using sol-gel electrophoretic deposition. Photocatalytic activity of nanostructured

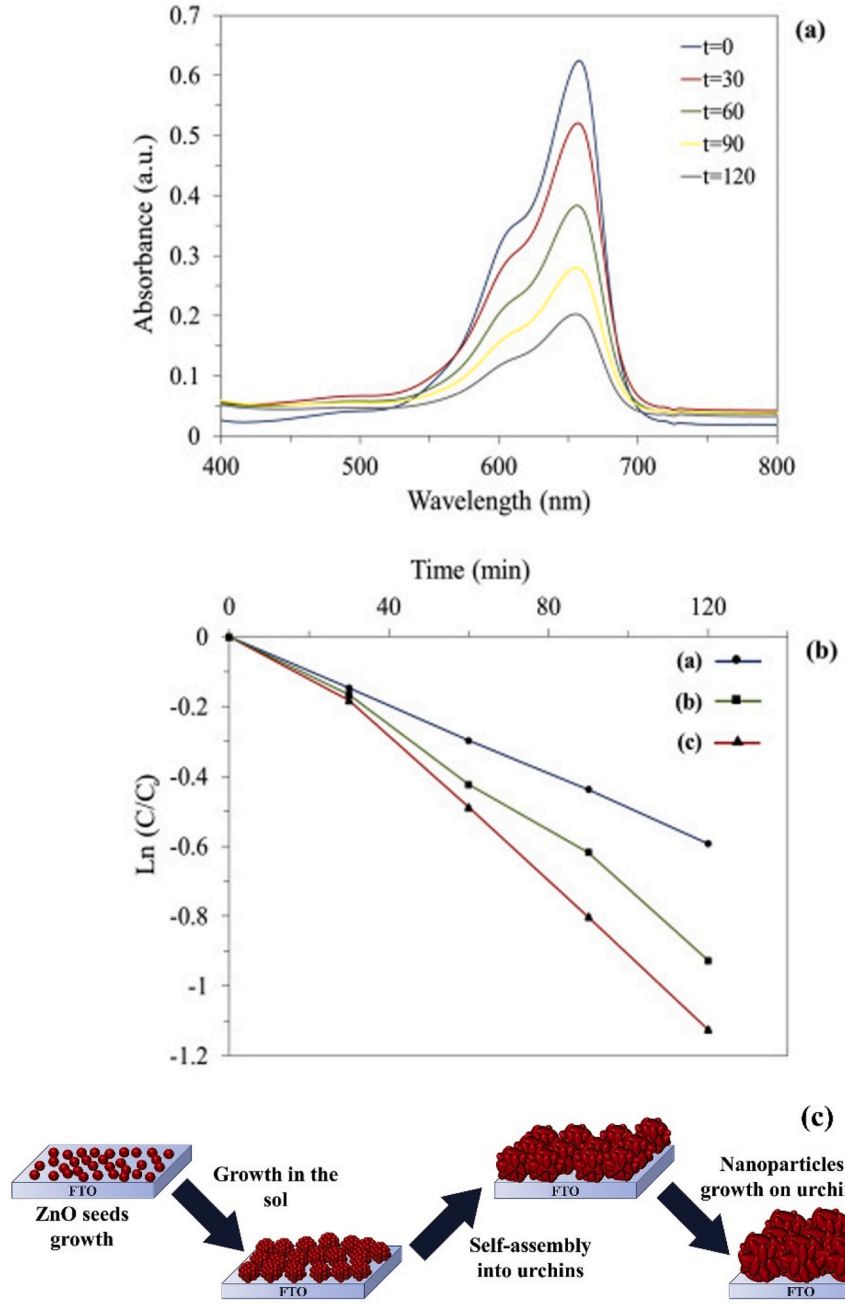

Fig. 16. (a) Time-dependency of methylene blue degradation in the presence of ZnO powder with urchin-like morphology under UV irradiation (initial concentration of methylene blue = 10^{-5} M). Reproduced with permission from Ref. [248] Copyright 2017 Elsevier. (b) Comparing the photocatalytic activity of ZnO powders with different morphologies ((a) in the absence of catalyst, (b) ZnO powder with irregular shaped nanoparticles, and (c) nanostructured ZnO powder with urchin-like morphology). Reproduced with permission from Ref. [248] Copyright 2017 Elsevier. (c) Schematic illustration of the formation of urchin-like ZnO films on FTO glass in the EPD process. Reproduced with permission from Ref. [248] Copyright 2017 Elsevier.

ZnO with urchin-like morphology and schematic illustration of the formation of urchin-like ZnO film using sol-gel EPD is shown in Fig. 16. It should be noted that to obtain powders, ZnO layers have been scraped off the substrate for evaluation of the photocatalytic activity.

Compared with traditional morphology, ZnO nanostructures with urchin-like morphology showed higher photocatalytic activity for the degradation of methylene blue which could be related to their large specific surface area, efficient light harvest, and efficient separation of charge carriers [248]. Navidpour et al. [249] fabricated ZnO films by EPD for the elimination of PFOA, where the addition of peroxymonosulfate (PMS) that can enable the production of sulfate radicals significantly improved PFOA removal. Notably, high PMS concentrations deteriorated the quality of ZnO coatings. It is also worth mentioning that the ZnO electrode fabricated at deposition time of 1 min provided the highest photocurrent response compared to those fabricated at deposition times of 2 min, 5 min, 10 min, and 20 min, signifying the key role of thickness and its optimization in photocatalytic/photoelectrocatalytic applications.

The advancements in tuning the orientation of deposited non-spherical materials could result in enhanced advantages of EPD over gaseous-based deposition processes. However, the formation of relatively thick films with good reproducibility and adhesion strength is essential for EPD to become a leading manufacturing method in some industries and applications [223].

6. Conclusions

Suspended nanoparticles have inherent limitations in the photocatalysis technology, despite their high specific surface area. Therefore, the immobilization of photocatalysts has received extensive attention. This research reviewed main immobilization techniques including PVD, spin coating, dip coating, spray pyrolysis, and EPD for the fabrication of TiO_2 and ZnO coatings for photocatalytic applications. Each deposition process possesses its advantages and disadvantages. Notably, processes like PVD are usually used for the deposition of thin films, whereas EPD could be used for the deposition of thick and thin films. Overall, among the various methods of surface engineering evaluated in this study, EPD with the capability of the fabrication of coatings with different morphologies and thicknesses is considered highly promising for photocatalytic applications. It is notable that EPD could reap the benefits of its advantages:

- None line of site coating method
- High deposition rate
- Low cost
- Simple apparatus
- High purity of the films
- High microstructure homogeneity of the films
- No need to binders/additives
- Creation of uniform coatings
- Capability of depositing porous microstructures
- Capability of using complex-shaped substrates
- Capability of using substrates with large surface areas
- Control over the film thickness
- Control over the coating structure

Although EPD is an industrial method of surface engineering, it suffers from the weak adhesion strength of films on their substrate, which can be improved by a post-heat treatment. In addition, the thickness of coatings should be optimized since ultra-thick films could suppress the photocatalytic performance. Therefore, certain strategies such as sintering and controlling the film thickness are necessary to increase the adhesion strength of the as-deposited films and to improve their proficiency in photocatalytic applications, respectively. These measures should facilitate the industrial applications of photocatalysis technology in wastewater treatment.

CRediT authorship contribution statement

Amir Hossein Navidpour: Writing – original draft, Investigation, Data curation. **Bentuo Xu:** Writing – review & editing. **Mohammad Boshir Ahmed:** Writing – review & editing. **John L. Zhou:** Writing – review & editing, Supervision.

Declaration of competing interest

The authors declare that they have no known competing financial interests or personal relationships that could have appeared to influence the work reported in this paper.

Data availability

Data will be made available on request.

Acknowledgments

This work was supported by the University of Technology Sydney.

References

[1] M.F. Hanafi, N. Sapawe, A review on the current techniques and technologies of organic pollutants removal from water/wastewater, Mater. Today: Proc. 31 (2020) A158–A165.
[2] Y. Deng, R. Zhao, Advanced oxidation processes (AOPs) in wastewater treatment, Curr. Pollut. Rep. 1 (2015) 167–176.
[3] D. Ma, H. Yi, C. Lai, X. Liu, X. Huo, Z. An, L. Li, Y. Fu, B. Li, M. Zhang, L. Qin, S. Liu, L. Yang, Critical review of advanced oxidation processes in organic wastewater treatment, Chemosphere 275 (2021) 130104.
[4] A. Bhambri, P. Singh, S.K. Karn, A. Dey, Chapter 8 - Agriculture pesticide and their remediation, in: M.P. Shah (Ed.), Development in Wastewater Treatment Research and Processes, Elsevier, 2023, pp. 145–162.
[5] S. Palit, C.M. Hussain, Chapter 2 - advanced oxidation processes as nonconventional environmental engineering techniques for water treatment and groundwater remediation, in: R.O.A. Rahman, C.M. Hussain (Eds.), Handbook of Advanced Approaches towards Pollution Prevention and Control, Elsevier, 2021, pp. 33–44.
[6] X. Yang, D. Wang, Photocatalysis: from fundamental principles to materials and applications, ACS Appl. Energy Mater. 1 (2018) 6657–6693.
[7] F. Zhang, X. Wang, H. Liu, C. Liu, Y. Wan, Y. Long, Z. Cai, Recent advances and applications of semiconductor photocatalytic technology, Appl. Sci. 9 (2019) 2489.
[8] A.H. Navidpour, M. Fakhrzad, M. Tahari, S. Abbasi, Novel photocatalytic coatings based on tin oxide semiconductor, Surf. Eng. 35 (2019) 216–226.
[9] A.H. Navidpour, M. Salehi, M. Amirnasr, H.R. Salimijazi, M. Azarpour Siahkali, Y. Kalantari, M. Mohammadnezhad, Photocatalytic iron oxide coatings produced by thermal spraying process, J. Therm. Spray Technol. 24 (2015) 1487–1497.
[10] A.H. Navidpour, M. Salehi, H.R. Salimijazi, Y. Kalantari, M. Azarpour Siahkali, Photocatalytic activity of flame-sprayed coating of zinc ferrite powder, J. Therm. Spray Technol. 26 (2017) 2030–2039.
[11] A.H. Navidpour, M. Fakhrzad, Photocatalytic and magnetic properties of $ZnFe_2O_4$ nanoparticles synthesised by mechanical alloying, Int. J. Environ. Anal. Chem. 102 (2022) 690–706.
[12] A.H. Navidpour, M. Fakhrzad, Photocatalytic activity of Zn_2SnO_4 coating deposited by air plasma spraying, Appl. Surf. Sci. Adv. 6 (2021) 100153.
[13] M. Fakhrzad, A.H. Navidpour, M. Tahari, S. Abbasi, Synthesis of Zn_2SnO_4 nanoparticles used for photocatalytic purposes, Mater. Res. Express 6 (2019) 095037.
[14] Navidpour, A.H.; Hao, D.; Li, X.; Li, D.; Huang, Z.; Zhou, J.L., Key factors in improving the synthesis and properties of visible-light activated g-C_3N_4 for photocatalytic hydrogen production and organic pollutant decomposition. Catal. Rev. ; [e-reference] https://doi.org/10.1080/01614940.2023.2228130.
[15] Y. Zhu, X. Liu, H. Liu, G. He, J. Xiao, H. Xie, Y. Sun, L. Han, Regulating nitrogen vacancies within graphitic carbon nitride to boost photocatalytic hydrogen peroxide production, SusMat 2 (2022) 617–629.
[16] A.H. Navidpour, S. Abbasi, D. Li, A. Mojiri, J.L. Zhou, Investigation of advanced oxidation process in the presence of TiO_2 semiconductor as photocatalyst: property, principle, kinetic analysis, and photocatalytic activity, Catalysts 13 (2023) 232.
[17] J. Chen, W. Zhang, H. Li, W. Li, D. Zhao, Recent advances in TiO_2-based catalysts for N_2 reduction reaction, SusMat 1 (2021) 174–193.
[18] A.H. Navidpour, Y. Kalantari, M. Salehi, H.R. Salimijazi, M. Amirnasr, M. Rismanchian, M. Azarpour Siahkali, Plasma-sprayed photocatalytic zinc oxide coatings, J. Therm. Spray Technol. 26 (2017) 717–727.
[19] A.H. Navidpour, J. Safaei, M.A.H. Johir, B.-J. Ni, A. Dashti, X. Li, J.L. Zhou, Zinc oxide@citric acid-modified graphitic carbon nitride nanocomposites for adsorption and photocatalytic degradation of perfluorooctanoic acid, Adv. Compos. Hybrid Mater. 7 (2024) 53.
[20] J. Arun, S. Nachiappan, G. Rangarajan, R.P. Alagappan, K.P. Gopinath, E. Lichtfouse, Synthesis and application of titanium dioxide photocatalysis for energy, decontamination and viral disinfection: a review, Environ. Chem. Lett. 21 (2023) 339–362.
[21] J. Gomes, J. Lincho, E. Domingues, R.M. Quinta-Ferreira, R.C. Martins, N–TiO_2 photocatalysts: a review of their characteristics and capacity for emerging contaminants removal, Water 11 (2019) 373.
[22] H.N. Dharma, J. Jaafar, N. Widiastuti, H. Matsuyama, S. Rajabsadeh, M. H. Othman, M.A. Rahman, N.N. Jafri, N.S. Suhaimin, A.M. Nasir, N.H. Alias, A review of titanium dioxide (TiO_2)-based photocatalyst for oilfield-produced water treatment, Membranes 12 (2022) 345.
[23] G.L. Chiarello, A. Di Paola, L. Palmisano, E. Selli, Effect of titanium dioxide crystalline structure on the photocatalytic production of hydrogen, Photochem. Photobiol. Sci. 10 (2011) 355–360.
[24] Y. Sun, W. Zhang, Q. Li, H. Liu, X. Wang, Preparations and applications of zinc oxide based photocatalytic materials, Adv. Sens. Energy Mater. 2 (2023) 100069.
[25] C.B. Ong, L.Y. Ng, A.W. Mohammad, A review of ZnO nanoparticles as solar photocatalysts: synthesis, mechanisms and applications, Renew. Sustain. Energy Rev. 81 (2018) 536–551.
[26] A.H. Navidpour, A. Hosseinzadeh, J.L. Zhou, Z. Huang, Progress in the application of surface engineering methods in immobilizing TiO_2 and ZnO coatings for environmental photocatalysis, Catal. Rev. 65 (2023) 822–873.
[27] S. Hernández, D. Hidalgo, A. Sacco, A. Chiodoni, A. Lamberti, V. Cauda, E. Tresso, G. Saracco, Comparison of photocatalytic and transport properties of TiO_2 and ZnO nanostructures for solar-driven water splitting, Phys. Chem. Chem. Phys. 17 (2015) 7775–7786.

[28] K.M. Mohamed, J.J. Benitto, J.J. Vijaya, M. Bououdina, Recent advances in ZnO-based nanostructures for the photocatalytic degradation of hazardous, non-biodegradable medicines, Crystals 13 (2023) 329.

[29] M.F.J. Dijkstra, A. Michorius, H. Buwalda, H.J. Panneman, J.G.M. Winkelman, A. A.C.M. Beenackers, Comparison of the efficiency of immobilized and suspended systems in photocatalytic degradation, Catal. Today 66 (2001) 487–494.

[30] G. Li, L. Lv, H. Fan, J. Ma, Y. Li, Y. Wan, X.S. Zhao, Effect of the agglomeration of TiO_2 nanoparticles on their photocatalytic performance in the aqueous phase, J. Colloid Interface Sci. 348 (2010) 342–347.

[31] F. Pellegrino, L. Pellutiè, F. Sordello, C. Minero, E. Ortel, V.-D. Hodoroaba, V. Maurino, Influence of agglomeration and aggregation on the photocatalytic activity of TiO_2 nanoparticles, Appl. Catal. B Environ. 216 (2017) 80–87.

[32] Z. Yu, H. Moussa, M. Liu, R. Schneider, W. Wang, M. Moliere, H. Liao, Development of photocatalytically active heterostructured MnO/ZnO and CuO/ZnO films via solution precursor plasma spray process, Surf. Coat. Technol. 371 (2019) 107–116.

[33] Z. Yu, H. Moussa, M. Liu, R. Schneider, M. Moliere, H. Liao, Heterostructured metal oxides-ZnO nanorods films prepared by SPPS route for photodegradation applications, Surf. Coat. Technol. 375 (2019) 670–680.

[34] Z. Yu, B. Chouchene, M. Liu, H. Moussa, R. Schneider, M. Moliere, H. Liao, Y. Chen, L. Sun, Influence of laminated architectures of heterostructured CeO_2-ZnO and Fe_2O_3-ZnO films on photodegradation performances, Surf. Coat. Technol. 403 (2020) 126367.

[35] J. Tian, L. Chen, Y. Yin, X. Wang, J. Dai, Z. Zhu, X. Liu, P. Wu, Photocatalyst of TiO_2/ZnO nano composite film: preparation, characterization, and photodegradation activity of methyl orange, Surf. Coat. Technol. 204 (2009) 205–214.

[36] A. Kleiman, J.M. Meichtry, D. Vega, M.I. Litter, A. Márquez, Photocatalytic activity of TiO_2 films prepared by cathodic arc deposition: dependence on thickness and reuse of the photocatalysts, Surf. Coat. Technol. 382 (2020) 125154.

[37] S. Veziroglu, M. Ullrich, M. Hussain, J. Drewes, J. Shondo, T. Strunskus, J. Adam, F. Faupel, O.C. Aktas, Plasmonic and non-plasmonic contributions on photocatalytic activity of Au-TiO_2 thin film under mixed UV–visible light, Surf. Coat. Technol. 389 (2020) 125613.

[38] M. Bozorgtabar, M. Rahimipour, M. Salehi, M. Jafarpour, Structure and photocatalytic activity of TiO_2 coatings deposited by atmospheric plasma spraying, Surf. Coat. Technol. 205 (2011) S229–S231.

[39] Y. Chen, C. Zhang, W. Huang, C. Yang, T. Huang, Y. Situ, H. Huang, Synthesis of porous ZnO/TiO_2 thin films with superhydrophilicity and photocatalytic activity via a template-free sol–gel method, Surf. Coat. Technol. 258 (2014) 531–538.

[40] V.B. Chintada, R. Koona, M.V.A. Raju Bahubalendruni, State of art review on nickel-based electroless coatings and materials, J. Bio- Tribo-Corros. 7 (2021) 134.

[41] M. Ramezani, Z. Mohd Ripin, T. Pasang, C.-P. Jiang, Surface engineering of metals: techniques, characterizations and applications, Metals 13 (2023) 1299.

[42] I. Hutchings, P. Shipway, Chapter 7 - surface engineering, in: I. Hutchings, P. Shipway (Eds.), Tribology, second ed., Butterworth-Heinemann, 2017, pp. 237–281.

[43] J. Dutta Majumdar, I. Manna, Chapter 21 - laser surface engineering of titanium and its alloys for improved wear, corrosion and high-temperature oxidation resistance, in: J. Lawrence, D.G. Waugh (Eds.), Laser Surface Engineering, Woodhead Publishing, 2015, pp. 483–521.

[44] J. Budida, K. Srinivasan, Review of thin film deposition and techniques, Mater. Today: Proc. 92 (2023) 1030–1033.

[45] N. White, Thick films, in: S. Kasap, P. Capper (Eds.), Springer Handbook of Electronic and Photonic Materials, Springer US, Boston, MA, 2007, pp. 717–731.

[46] E.B. Gutoff, E.D. Cohen, Chapter 13 - water- and solvent-based coating technology, in: J.R. Wagner (Ed.), Multilayer Flexible Packaging, William Andrew Publishing, Boston, 2010, pp. 163–184.

[47] İ. Ucun, K. Aslantaş, B. Gökçe, F. Bedir, Effect of tool coating materials on surface roughness in micromachining of Inconel 718 super alloy, Proc. Inst. Mech. Eng. B: J. Eng. Manuf. 228 (2014) 1550–1562.

[48] B. Bhushan, Surface roughness analysis and measurement techniques, in: B. Bhushan (Ed.), Modern Tribology Handbook, Two Volume Set, CRC Press, 2000, pp. 79–150.

[49] T.S. Dörr, L. Deilmann, G. Haselmann, A. Cherevan, P. Zhang, P. Blaha, P.W. de Oliveira, T. Kraus, D. Eder, Ordered mesoporous TiO_2 gyroids: effects of pore architecture and Nb-doping on photocatalytic hydrogen evolution under UV and visible irradiation, Adv. Energy Mater. 8 (2018) 1802566.

[50] N.X. Qian, X. Zhang, M. Wang, X. Sun, X.Y. Sun, C. Liu, R. Rao, Y.Q. Ma, Great enhancement in photocatalytic performance of (001)-TiO_2 through N-doping via the vapor-thermal method, J. Photochem. Photobiol., A: Chem 386 (2020) 112127.

[51] M.L. García-Benjume, M.I. Espitia-Cabrera, M.E. Contreras-García, Enhanced photocatalytic activity of hierarchical macro-mesoporous anatase by ZrO_2 incorporation, Int. J. Photoenergy 2012 (2012) 609561.

[52] H. Liu, Y. Zhang, H. Yang, W. Xiao, L. Sun, Study on synthesis and photocatalytic activity of porous titania nanotubes, Adv. Mater. Sci. Eng. 2016 (2016) 3532817.

[53] K. He, C. Zhao, G. Zhao, G. Han, Effects of pore size on the photocatalytic activity of mesoporous TiO_2 prepared by a sol–gel process, J. Sol. Gel Sci. Technol. 75 (2015) 557–563.

[54] J. Yu, X. Zhao, Q. Zhao, Effect of film thickness on the grain size and photocatalytic activity of the sol–gel derived nanometer TiO_2 thin films, J. Mater. Sci. Lett. 19 (2000) 1015–1017.

[55] Z.R. Rivera, A.M. Alvarez, M.d.l.L.O. Amador, Effect of thickness on photocatalytic properties of ZnO thin films deposited by RF magnetron sputtering, in: Proceedings of the 2019 16th International Conference on Electrical Engineering, Computing Science and Automatic Control (CCE), 2019, pp. 1–6.

[56] N. Kaneva, A. Bojinova, K. Papazova, D. Dimitrov, I. Svinyarov, M. Bogdanov, Effect of thickness on the photocatalytic properties of ZnO thin films, Bulg. Chem. Commun. 47 (2015) 395–401.

[57] M. Barthomeuf, X. Castel, L. Le Gendre, J. Louis, M. Denis, C. Pissavin, Effect of titanium dioxide film thickness on photocatalytic and bactericidal activities against listeria monocytogenes, Photochem. Photobiol. 95 (2019) 1035–1044.

[58] Y.-H. Chen, K.-J. Tu, Thickness dependent on photocatalytic activity of hematite thin films, Int. J. Photoenergy 2012 (2012) 980595.

[59] W.X. Xianyu, M.K. Park, W.I. Lee, Thickness effect in the photocatalytic activity of TiO_2 thin films derived from sol-gel process, Kor. J. Chem. Eng. 18 (2001) 903–907.

[60] M. Aleksandrzak, P. Adamski, W. Kukułka, B. Zielinska, E. Mijowska, Effect of graphene thickness on photocatalytic activity of TiO_2-graphene nanocomposites, Appl. Surf. Sci. 331 (2015) 193–199.

[61] I. Dundar, A. Mere, V. Mikli, M. Krunks, I. Oja Acik, Thickness effect on photocatalytic activity of TiO_2 thin films fabricated by ultrasonic spray pyrolysis, Catalysts 10 (2020) 1058.

[62] T.W. Boentoro, B. Szyszka, Chapter 14 - Protective coatings for optical surfaces, in: A. Piegari, F. Flory (Eds.), Optical Thin Films and Coatings, Woodhead Publishing, 2013, pp. 540–563.

[63] Q. Wei, Y. Xu, Y. Wang, Chapter 3 - Textile surface functionalization by physical vapor deposition (PVD), in: Q. Wei (Ed.), Surface Modification of Textiles, Woodhead Publishing, 2009, pp. 58–90.

[64] M. Łach, G. Róg, K. Ochman, K. Pławecka, A. Bąk, K. Korniejenko, Assessment of adhesion of geopolymer and varnished coatings by the pull-off method, Engineer 3 (2022) 42–59.

[65] D. Wolfe, T. Eden, Chapter 14 - Cold spray particle deposition for improved wear resistance, in: V.K. Champagne (Ed.), The Cold Spray Materials Deposition Process, Woodhead Publishing, 2007, pp. 264–301.

[66] T.-G. Wang, Y. Liu, Q. Wang, J. Gong, C. Sun, K.H. Kim, Influence of residual stress on the adhesive behavior of detonation gun sprayed WC–Co coatings, Curr. Appl. Phys. 12 (2012) S59–S62.

[67] R. Ali, M. Renzelli, I.M. Khan, M. Sebastiani, E. Bemporad, Effects of residual stress distribution on interfacial adhesion of magnetron sputtered AlN and AlN/Al nanostructured coatings on a (100) silicon substrate, Nanomaterials 8 (2018) 896.

[68] M. Aliofkhazraei, N. Ali, 7.04 - PVD technology in fabrication of micro- and nanostructured coatings, in: S. Hashmi, G.F. Batalha, C.J. Van Tyne, B. Yilbas (Eds.), Comprehensive Materials Processing, Elsevier, Oxford, 2014, pp. 49–84.

[69] D.M. Mattox, Chapter 1 - Introduction, in: D.M. Mattox (Ed.), Handbook of Physical Vapor Deposition (PVD) Processing, second ed., William Andrew Publishing, Boston, 2010, pp. 1–24.

[70] R. Dorey, Chapter 2 - Routes to thick films: what is a thick film? How is it made? in: R. Dorey (Ed.), Ceramic Thick Films for MEMS and Microdevices William Andrew Publishing, Oxford, 2012, pp. 35–61.

[71] A.V. Rane, K. Kanny, V.K. Abitha, S. Thomas, Chapter 5 - methods for synthesis of nanoparticles and fabrication of nanocomposites, in: S. Mohan Bhagyaraj, O.S. Oluwafemi, N. Kalarikkal, S. Thomas (Eds.), Synthesis of Inorganic Nanomaterials, Woodhead Publishing2018, pp. 121-139..

[72] D.M. Mattox, Chapter 3 - the “good” vacuum (low pressure) processing environment, in: D.M. Mattox (Ed.), Handbook of Physical Vapor Deposition (PVD) Processing, second ed., William Andrew Publishing, Boston, 2010, pp. 73–145.

[73] M.S. Zafar, I. Farooq, M. Awais, S. Najeeb, Z. Khurshid, S. Zohaib, Chapter 11 - bioactive surface coatings for enhancing osseointegration of dental implants, in: G. Kaur (Ed.), Biomedical, Therapeutic and Clinical Applications of Bioactive Glasses, Woodhead Publishing, 2019, pp. 313–329.

[74] A.S.H. Makhlouf, Chapter 1 - current and advanced coating technologies for industrial applications, in: A.S.H. Makhlouf, I. Tiginyanu (Eds.), Nanocoatings and Ultra-thin Films, Woodhead Publishing, 2011, pp. 3–23.

[75] J.A. Juhasz, S.M. Best, Chapter 6 - surface modification of biomaterials by calcium phosphate deposition, in: R. Williams (Ed.), Surface Modification of Biomaterials, Woodhead Publishing, 2011, pp. 143–169.

[76] H. Adachi, K. Wasa, Chapter 1 - thin films and nanomaterials, in: K. Wasa, I. Kanno, H. Kotera (Eds.), Handbook of Sputtering Technology, second ed., William Andrew Publishing, Oxford, 2012, pp. 3–39.

[77] A. Bashir, T.I. Awan, A. Tehseen, M.B. Tahir, M. Ijaz, Chapter 3 - interfaces and surfaces, in: T.I. Awan, A. Bashir, A. Tehseen (Eds.), Chemistry of Nanomaterials, Elsevier, 2020, pp. 51–87.

[78] S.J.C. Irvine, Film growth and epitaxy methods, in: T. Chakraborty (Ed.), Encyclopedia of Condensed Matter Physics, second ed., Academic Press, Oxford, 2024, pp. 248–260.

[79] R. Luttge, Chapter 2 - Basic technologies for microsystems, in: R. Luttge (Ed.), Microfabrication for Industrial Applications, William Andrew Publishing, Boston, 2011, pp. 13–54.

[80] J. Shinar, R. Shinar, 1.04 - an overview of organic light-emitting diodes and their applications, in: D.L. Andrews, G.D. Scholes, G.P. Wiederrecht (Eds.), Comprehensive Nanoscience and Technology, Academic Press, Amsterdam, 2011, pp. 73–107.

[81] A. Taherniya, D. Raoufi, The annealing temperature dependence of anatase TiO_2 thin films prepared by the electron-beam evaporation method, Semicond. Sci. Technol. 31 (2016) 125012.
[82] S.H. Oh, D.J. Kim, S.H. Hahn, E.J. Kim, Comparison of optical and photocatalytic properties of TiO_2 thin films prepared by electron-beam evaporation and sol–gel dip-coating, Mater. Lett. 57 (2003) 4151–4155.
[83] W. Qiu, U.W. Paetzold, R. Gehlhaar, V. Smirnov, H.-G. Boyen, J.G. Tait, B. Conings, W. Zhang, C.B. Nielsen, I. McCulloch, L. Froyen, P. Heremans, D. Cheyns, An electron beam evaporated TiO_2 layer for high efficiency planar perovskite solar cells on flexible polyethylene terephthalate substrates, J. Mater. Chem. A 3 (2015) 22824–22829.
[84] Ö. Duyar, F. Placido, H. Zafer Durusoy, Optimization of TiO_2 films prepared by reactive electron beam evaporation of Ti_3O_5, J. Phys. D Appl. Phys. 41 (2008) 095307.
[85] A. Khoury, R. al Asmar, M. Abdallah, G.E.H. Moussa, A. Foucaran, Comparative study between zinc oxide elaborated by spray pyrolysis, electron beam evaporation and rf magnetron techniques, Phys. Status Solidi (A) Appl. Mater. Sci. 207 (2010) 1900–1904.
[86] N. Yamaguchi, T. Kuroyama, Y. Okuhara, H. Matsubara, Properties of Al doped zinc oxide films prepared by electron beam-PVD, IOP Conf. Ser. Mater. Sci. Eng. 18 (2011) 092025.
[87] P.K. Giri, P.K. Patel, C.J. Panchal, S. Bhattacharyya, S. Kumari, D.K. Singh, V. A. Kheraj, N.M. Shah, P.D. Vakil, K.J. Patel, M.S. Desai, B. Rehani, V.J. Rao, R. R. Desai, D. Lakshminarayana, P.B. Patel, Studies on zinc oxide nanorods grown by electron beam evaporation technique, Synth. React. Inorg., Met.-Org., Nano-Met. Chem. 37 (2007) 437–441.
[88] J.K. Yao, H.L. Huang, J.Y. Ma, Y.X. Jin, Y.A. Zhao, J.D. Shao, H.B. He, K. Yi, Z. X. Fan, F. Zhang, Z.Y. Wu, High refractive index TiO_2 film deposited by electron beam evaporation, Surf. Eng. 25 (2013) 257–260.
[89] B. Scheffel, T. Modes, C. Metzner, Reactive high-rate deposition of titanium oxide coatings using electron beam evaporation, spotless arc and dual crucible, Surf. Coat. Technol. 287 (2016) 138–144.
[90] A. Taherniya, D. Raoufi, The annealing temperature dependence of anatase TiO_2 thin films prepared by the electron-beam evaporation method, Semicond. Sci. Technol. 31 (2016) 125012.
[91] N. An, K. Wang, H. Wei, Q. Song, S. Xiao, Fabricating high refractive index titanium dioxide film using electron beam evaporation for all-dielectric metasurfaces, MRS Commun 6 (2016) 77–83.
[92] R. van de Krol, A. Goossens, Structure and properties of anatase TiO_2 thin films made by reactive electron beam evaporation, J. Vac. Sci. Technol. A 21 (2002) 76–83.
[93] M.H. Mangrola, V.G. Joshi, Synthesis, characterization and study of influence of pure TiO_2 nanoparticles thin film developed by e-beam evaporation, Mater, Today Off.: SAVE Proc. 4 (2017) 3832–3841.
[94] A. Zaier, A. Meftah, A.Y. Jaber, A.A. Abdelaziz, M.S. Aida, Annealing effects on the structural, electrical and optical properties of ZnO thin films prepared by thermal evaporation technique, J. King Saud Univ. Sci. 27 (2015) 356–360.
[95] R. Al Asmar, G. Ferblantier, F. Mailly, P. Gall-Borrut, A. Foucaran, Effect of annealing on the electrical and optical properties of electron beam evaporated ZnO thin films, Thin Solid Films 473 (2005) 49–53.
[96] C. Periasamy, R. Prakash, P. Chakrabarti, Effect of post annealing on structural and optical properties of ZnO thin films deposited by vacuum coating technique, J. Mater. Sci. Mater. Electron. 21 (2010) 309–315.
[97] D.R. Sahu, S.-Y. Lin, J.-L. Huang, Improved properties of Al-doped ZnO film by electron beam evaporation technique, Microelectron. J. 38 (2007) 245–250.
[98] R. Al Asmar, D. Zaouk, P. Bahouth, J. Podleki, A. Foucaran, Characterization of electron beam evaporated ZnO thin films and stacking ZnO fabricated by e-beam evaporation and rf magnetron sputtering for the realization of resonators, Microelectron. Eng. 83 (2006) 393–398.
[99] A. Kuroyanagi, Properties of aluminum-doped ZnO thin films grown by electron beam evaporation, Jpn. J. Appl. Phys. 28 (1989) 219–222.
[100] D.C. Agarwal, R.S. Chauhan, A. Kumar, D. Kabiraj, F. Singh, S.A. Khan, D. K. Avasthi, J.C. Pivin, M. Kumar, J. Ghatak, P.V. Satyam, Synthesis and characterization of ZnO thin film grown by electron beam evaporation, J. Appl. Phys. 99 (2006) 123105.
[101] V.D. Falcao, M.E.L. Sabino, D.O. Miranda, A.S.A.C. Diniz, J.R.T. Branco, Transparent conducting zinc oxide thin film prepared by electron beam evaporation technique with argon plasma assistance, in: Proceedings of the 2008 33rd IEEE Photovoltaic Specialists Conference, 2008, pp. 1–3.
[102] V. Gupta, K. Sreenivas, M. Fahim, Influence of interstitial oxygen on the c-axis orientation of sputtered and e-beam evaporated ZnO thin films, ISAF 1998. Proceedings of the Eleventh IEEE International Symposium on Applications of Ferroelectrics (Cat. No.98CH36245), 1998, pp. 325–328.
[103] V.D. Falcão, D.O. Miranda, M.E.L. Sabino, T.D.O. Moura, A.S.A.C. Diniz, L. R. Cruz, J.R.T. Branco, Comparative study of ZnO thin films prepared by plasma deposition and electron beam evaporation for use in photovoltaic devices, Prog. Photovoltaics Res. Appl. 19 (2011) 149–154.
[104] D. Depla, S. Mahieu, J.E. Greene, Chapter 5 - sputter deposition processes, in: P. M. Martin (Ed.), Handbook of Deposition Technologies for Films and Coatings, third ed., William Andrew Publishing, Boston, 2010, pp. 253–296.
[105] A. Sarangan, Chapter 5 - Nanofabrication, in: J.W. Haus (Ed.), Fundamentals and Applications of Nanophotonics, Woodhead Publishing, 2016, pp. 149–184.
[106] F. Wang, J. Wu, Chapter 8 - magnetron sputtering, in: F. Wang, J. Wu (Eds.), Modern Ion Plating Technology, Elsevier, 2023, pp. 189–228.
[107] V. Teixeira, J. Carneiro, P. Carvalho, E. Silva, S. Azevedo, C. Batista, Chapter 11 - high barrier plastics using nanoscale inorganic films, in: J.-M. Lagarón (Ed.), Multifunctional and Nanoreinforced Polymers for Food Packaging, Woodhead Publishing, 2011, pp. 285–315.
[108] D.M. Mattox, Chapter 7 - physical sputtering and sputter deposition (sputtering), in: D.M. Mattox (Ed.), Handbook of Physical Vapor Deposition (PVD) Processing, second ed., William Andrew Publishing, Boston, 2010, pp. 237–286.
[109] A. Zhou, Chapter 2 - methods of MAX-phase synthesis and densification – II, in: I. M. Low (Ed.), Advances in Science and Technology of Mn+1AXn Phases, Woodhead Publishing, 2012, pp. 21–46.
[110] R. Wördenweber, 4.06 - Ferroelectric thin layers, in: P. Bhattacharya, R. Fornari, H. Kamimura (Eds.), Comprehensive Semiconductor Science and Technology, Elsevier, Amsterdam, 2011, pp. 177–205.
[111] A. Shrivastava, Chapter 3 - plastic properties and testing, in: A. Shrivastava (Ed.), Introduction to Plastics Engineering, William Andrew Publishing, 2018, pp. 49–110.
[112] W.D. Sproul, D.J. Christie, D.C. Carter, Control of reactive sputtering processes, Thin Solid Films 491 (2005) 1–17.
[113] S. Berg, T. Nyberg, T. Kubart, Modelling of reactive sputtering processes, in: D. Depla, S. Mahieu (Eds.), Reactive Sputter Deposition, Springer Berlin Heidelberg, Berlin, Heidelberg, 2008, pp. 131–152.
[114] S. Boyadzhiev, V. Georgieva, M. Rassovska, Characterization of reactive sputtered TiO_2 thin films for gas sensor applications, J. Phys.: Conf. Ser. 253 (2010) 012040.
[115] C. Guillén, J. Herrero, TiO_2 coatings obtained by reactive sputtering at room temperature: physical properties as a function of the sputtering pressure and film thickness, Thin Solid Films 636 (2017) 193–199.
[116] E. Mirica, G. Kowach, P. Evans, H. Du, Morphological evolution of ZnO thin films deposited by reactive sputtering, Cryst. Growth Des. 4 (2004) 147–156.
[117] Z. Li, W. Gao, ZnO thin films with DC and RF reactive sputtering, Mater. Lett. 58 (2004) 1363–1370.
[118] G. Faraji, H.S. Kim, H.T. Kashi, Introduction, in: G. Faraji, H.S. Kim, H.T. Kashi (Eds.), Severe Plastic Deformation, Elsevier, 2018, pp. 1–17.
[119] D.A. Lamprou, N. Scoutaris, S.A. Ross, D. Douroumis, Polymeric coatings and their fabrication for medical devices, in: R. Narayan (Ed.), Encyclopedia of Biomedical Engineering, Elsevier, Oxford, 2019, pp. 177–187.
[120] G.P. Halada, C.R. Clayton, Chapter 15 - the intersection of design, manufacturing, and surface engineering, in: M. Kutz (Ed.), Handbook of Environmental Degradation of Materials, second ed., William Andrew Publishing, Oxford, 2012, pp. 443–480.
[121] R.J. Martín-Palma, A. Lakhtakia, Chapter 15 - vapor-deposition techniques, in: A. Lakhtakia, R.J. Martín-Palma (Eds.), Engineered Biomimicry, Elsevier, Boston, 2013, pp. 383–398.
[122] I. Bozovic, D.G. Schlom, Superconducting thin films: materials, preparation, and properties, in: K.H.J. Buschow, R.W. Cahn, M.C. Flemings, B. Ilschner, E. J. Kramer, S. Mahajan, P. Veyssière (Eds.), Encyclopedia of Materials: Science and Technology, Elsevier, Oxford, 2001, pp. 8955–8964.
[123] A.J. Hadi, U.M. Nayef, F.A.H. Mutlak, M.S. Jabir, High-efficiency photodetectors based on zinc oxide nanostructures on porous silicon grown by pulsed laser deposition, Plasmonics 19 (2024) 577–593.
[124] R.B. Ettlinger, A. Cazzaniga, S. Canulescu, N. Pryds, J. Schou, Pulsed laser deposition from ZnS and Cu_2SnS_3 multicomponent targets, Appl. Surf. Sci. 336 (2015) 385–390.
[125] J. Schou, M. Gansukh, R.B. Ettlinger, A. Cazzaniga, M. Grossberg, M. Kauk-Kuusik, S. Canulescu, Pulsed laser deposition of chalcogenide sulfides from multi- and single-component targets: the non-stoichiometric material transfer, Appl. Phys. A 124 (2018) 78.
[126] M. Tyunina, J. Levoska, S. Leppävuori, Sorption in pulsed laser deposition of multicomponent materials: experiment versus modeling, J. Appl. Phys. 86 (1999) 2901–2908.
[127] D. Fischer, G. de la Fuente, A new pulsed laser deposition technique: scanning multi-component pulsed laser deposition method, Rev. Sci. Instrum. 83 (2012) 043901.
[128] T. Luttrell, S. Halpegamage, E. Sutter, M. Batzill, Photocatalytic activity of anatase and rutile TiO_2 epitaxial thin film grown by pulsed laser deposition, Thin Solid Films 564 (2014) 146–155.
[129] M. Cesaria, L. Scrimieri, A. Torrisi, G. Quarta, A. Serra, D. Manno, A.P. Caricato, M. Martino, L. Calcagnile, L. Velardi, Pulsed-laser deposition and photocatalytic activity of pure rutile and anatase TiO_2 films: impact of single-phased target and deposition conditions, Vacuum 202 (2022) 111150.
[130] J. Hu, H. Tang, X. Lin, Z. Luo, H. Cao, Q. Li, Y. Liu, J. Long, P. Wang, Doped titanium dioxide films prepared by pulsed laser deposition method, Int. J. Photoenergy 2012 (2012) 758539.
[131] N. Yudasari, D.S. Kennedy, M.M. Suliyanti, Pulse laser deposition (PLD) technique for ZnO photocatalyst fabrication, J. Phys.: Conf. Ser. 1191 (2019) 012009.
[132] G. Li, B. Sun, Y. Wang, Z. Wu, W. Zhang, Origin of difference in photocatalytic activity of ZnO (002) grown on a- and c-face sapphire, Int. J. Photoenergy 2014 (2014) 135725.
[133] T. Yamaki, T. Sumita, S. Yamamoto, A. Miyashita, Preparation of epitaxial TiO_2 films by PLD for photocatalyst applications, J. Cryst. Growth 237–239 (2002) 574–579.
[134] I. Brandt, C. Plá Cid, C. Azevedo, A.L.J. Pereira, L. Benetti, A.s. Ferlauto, J.H.D. da Silva, A. Pasa, Influence of substrate on the structure of predominantly anatase TiO_2 films grown by reactive sputtering, RSC Adv. 8 (2018) 7062–7071.
[135] H. Sakama, G. Osada, M. Tsukamoto, A. Tanokura, N. Ichikawa, Epitaxial growth of anatase TiO_2 thin films on LaAlO3(100) prepared using pulsed laser deposition, Thin Solid Films 515 (2006) 535–539.

[136] M. Zhu, T. Chikyow, P. Ahmet, T. Naruke, M. Murakami, Y. Matsumoto, H. Koinuma, A high-resolution transmission electron microscopy investigation of the microstructure of TiO_2 anatase film deposited on LaAlO3 and SrTiO3 substrates by laser ablation, Thin Solid Films 441 (2003) 140–144.
[137] K. Krupski, A.M. Sanchez, A. Krupski, C.F. McConville, Optimisation of anatase TiO_2 thin film growth on LaAlO3(0 0 1) using pulsed laser deposition, Appl. Surf. Sci. 388 (2016) 684–690.
[138] B.H. Park, J.Y. Huang, L.S. Li, Q.X. Jia, Role of atomic arrangements at interfaces on the phase control of epitaxial TiO_2 films, Appl. Phys. Lett. 80 (2002) 1174–1176.
[139] R. Shinohara, T. Yamaki, S. Yamamoto, H. Itoh, K. Asai, High-quality epitaxial TiO_2 thin films grown on α-Al_2O_3 substrates by pulsed laser deposition, J. Mater. Sci. Lett. 21 (2002) 967–969.
[140] S. Rout, N. Popovici, S. Dalui, M.L. Paramês, R.C. da Silva, A.J. Silvestre, O. Conde, Phase growth control in low temperature PLD Co: TiO_2 films by pressure, Curr. Appl. Phys. 13 (2013) 670–676.
[141] A. Gordienko, A.B. Kaye, Unique pulsed-laser deposition production of anatase and rutile TiO_2 on Al_2O_3, Cryst. Struct. Theor. Appl. 7 (2018) 19–31.
[142] H. Lin, A.K. Rumaiz, M. Schulz, D. Wang, R. Rock, C.P. Huang, S.I. Shah, Photocatalytic activity of pulsed laser deposited TiO_2 thin films, Mater. Sci. Eng. B 151 (2008) 133–139.
[143] N. Inoue, H. Yuasa, M. Okoshi, TiO_2 thin films prepared by PLD for photocatalytic applications, Appl. Surf. Sci. 197–198 (2002) 393–397.
[144] L. Zhao, J.-s. Lian, Effect of substrate temperature on structural properties and photocatalytic activity of TiO_2 thin films, Trans. Nonferrous Metals Soc. China 17 (2007) 772–776.
[145] J.-P. Mosnier, R.J. O'Haire, E. McGlynn, M.O. Henry, S.J. McDonnell, M.A. Boyle, K.G. McGuigan, ZnO films grown by pulsed-laser deposition on soda lime glass substrates for the ultraviolet inactivation of Staphylococcus epidermidis biofilms, Sci. Technol. Adv. Mater. 10 (2009) 045003.
[146] J. He, H. Zhuang, C. Xue, S. Wang, L. Hu, S. Xue, Effect of substrate temperature on microstructural and optical properties of ZnO films grown by pulsed laser deposition, Rare Met. 25 (2006) 161–165.
[147] Y. Zhao, Y. Jiang, Y. Fang, The influence of substrate temperature on ZnO thin films prepared by PLD technique, J. Cryst. Growth 307 (2007) 278–282.
[148] E. Abdel-Fattah, I.A. Elsayed, T. Fahmy, Substrate temperature and laser fluence effects on properties of ZnO thin films deposited by pulsed laser deposition, J. Mater. Sci. Mater. Electron. 29 (2018) 19942–19950.
[149] J. Chang, Y.L. Zhou, Y. Zhou, Chapter 2 - surface modification of bioactive glasses, in: H.O. Ylänen (Ed.), Bioactive Glasses, Woodhead Publishing, 2011, pp. 29–52.
[150] M.C. Rao, Pulsed laser deposition - ablation mechanism and applications, Int. J. Mod. Phys.: Conf. Ser. 22 (2013) 355–360.
[151] P. Kuppusami, V.S. Raghunathan, Status of pulsed laser deposition: challenges and opportunities, Surf. Eng. 22 (2013) 81–83.
[152] S.S. Manjunatha, S. Basavarajappa, Effect of coating thickness on properties of Mo coatings deposited by plasma spraying, Tribol. Mater. Surface Interfac. 9 (2015) 41–45.
[153] W. Winarto, N. Sofyan, D. Rooscote, Porosity and wear resistance of flame sprayed tungsten carbide coatings, AIP Conf. Proc. 1855 (2017) 030012.
[154] J. Orava, T. Kohoutek, T. Wagner, Chapter 9 - deposition techniques for chalcogenide thin films, in: J.-L. Adam, X. Zhang (Eds.), Chalcogenide Glasses, Woodhead Publishing, 2014, pp. 265–309.
[155] I.W. Boyd, Thin film growth by pulsed laser deposition, Ceram. Int. 22 (1996) 429–434.
[156] D. Benetti, R. Nouar, R. Nechache, H. Pepin, A. Sarkissian, F. Rosei, J. M. MacLeod, Combined magnetron sputtering and pulsed laser deposition of TiO_2 and BFCO thin films, Sci. Rep. 7 (2017) 2503.
[157] A. Baptista, F. Silva, J. Porteiro, J. Míguez, G. Pinto, Sputtering physical vapour deposition (PVD) coatings: a critical review on process improvement and market trend demands, Coatings 8 (2018) 402.
[158] L. Xie, D. Abliz, D. Li, 7.07 - thin film coating for polymeric micro parts, in: S. Hashmi, G.F. Batalha, C.J. Van Tyne, B. Yilbas (Eds.), Comprehensive Materials Processing, Elsevier, Oxford, 2014, pp. 157–170.
[159] A. Mohammadzadeh, S.K. Naghib Zadeh, M.H. Saidi, M. Sharifzadeh, Chapter 3 - mechanical engineering of solid oxide fuel cell systems: geometric design, mechanical configuration, and thermal analysis, in: M. Sharifzadeh (Ed.), Design and Operation of Solid Oxide Fuel Cells, Academic Press, 2020, pp. 85–130.
[160] X. Tang, X. Yan, Dip-coating for fibrous materials: mechanism, methods and applications, J. Sol. Gel Sci. Technol. 81 (2017) 378–404.
[161] M. Aslan Çakır, T. Yetim, A.F. Yetim, A. Çelik, Superamphiphobic TiO_2 film by sol–gel dip coating method on commercial pure titanium, J. of Materi. Eng. and Perform. 33 (2024) 1472–1484.
[162] S. Sakka, Preparation and properties of sol-gel coating films, J. Sol. Gel Sci. Technol. 2 (1994) 451–455.
[163] M.M. Khalaf, H.M. Abd El-Lateef, Corrosion protection of mild steel by coating with TiO_2 thin films co-doped with NiO and ZrO_2 in acidic chloride environments, Mater. Chem. Phys. 177 (2016) 250–265.
[164] Y. Morimoto, K. Abe, Effect of additives in precursor solution on ZnO thin-film deposition by sol–gel dip-coating method, Jpn. J. Appl. Phys. 59 (2019) SAAC07.
[165] Y. Liang, S. Sun, T. Deng, H. Ding, W. Chen, Y. Chen, The preparation of TiO_2 film by the sol-gel method and evaluation of its self-cleaning property, Materials 11 (2018) 450.
[166] W.A. Thompson, C. Perier, M.M. Maroto-Valer, Systematic study of sol-gel parameters on TiO_2 coating for CO_2 photoreduction, Appl. Catal. B Environ. 238 (2018) 136–146.
[167] S.S. Pathak, A.S. Khanna, Chapter 12 - sol–gel nanocoatings for corrosion protection, in: V.S. Saji, R. Cook (Eds.), Corrosion Protection and Control Using Nanomaterials, Woodhead Publishing, 2012, pp. 304–329.
[168] P. Choudhury, D.C. Agrawal, Chapter 5 - hydroxyapatite (HA) coatings for biomaterials, in: T.J. Webster (Ed.), Nanomedicine, Woodhead Publishing, 2012, pp. 84–127.
[169] E. Blanco, J.M. González-Leal, M. Ramírez-del Solar, Photocatalytic TiO_2 sol–gel thin films: optical and morphological characterization, Sol. Energy 122 (2015) 11–23.
[170] S.K. Sahoo, B. Manoharan, N. Sivakumar, Chapter 1 - introduction: Why perovskite and perovskite solar cells? in: S. Thomas, A. Thankappan (Eds.), Perovskite Photovoltaics Academic Press, 2018, pp. 1–24.
[171] K. Kakaei, M.D. Esrafili, A. Ehsani, Chapter 8 - graphene and anticorrosive properties, in: K. Kakaei, M.D. Esrafili, A. Ehsani (Eds.), Interface Science and Technology, Elsevier, 2019, pp. 303–337.
[172] S. Obregón, V. Rodríguez-González, Photocatalytic TiO_2 thin films and coatings prepared by sol–gel processing: a brief review, J. Sol. Gel Sci. Technol. 102 (2022) 125–141.
[173] M. Aymerich, A. Gómez-Varela, E. Álvarez, M. Flores-Arias, Study of different sol-gel coatings to enhance the lifetime of PDMS devices: evaluation of their biocompatibility, Materials 9 (2016) 728.
[174] K.A. Kravanja, M. Finšgar, A review of techniques for the application of bioactive coatings on metal-based implants to achieve controlled release of active ingredients, Mater. Des. 217 (2022) 110653.
[175] A. Bouarioua, M. Zerdaoui, Photocatalytic activities of TiO_2 layers immobilized on glass substrates by dip-coating technique toward the decolorization of methyl orange as a model organic pollutant, J. Environ. Chem. Eng. 5 (2017) 1565–1574.
[176] V. Vaiano, O. Sacco, D. Sannino, P. Ciambelli, Nanostructured N-doped TiO_2 coated on glass spheres for the photocatalytic removal of organic dyes under UV or visible light irradiation, Appl. Catal. B Environ. 170–171 (2015) 153–161.
[177] Z. Hamden, S. Boufi, D.S. Conceição, A.M. Ferraria, A.M.B. do Rego, D.P. Ferreira, L.F.V. Ferreira, S. Bouattour, Li–N doped and codoped TiO_2 thin films deposited by dip-coating: characterization and photocatalytic activity under halogen lamp, Appl. Surf. Sci. 314 (2014) 910–918.
[178] K. Thongsuriwong, P. Amornpitoksuk, S. Suwanboon, Structure, morphology, photocatalytic and antibacterial activities of ZnO thin films prepared by sol–gel dip-coating method, Adv. Powder Technol. 24 (2013) 275–280.
[179] M. Toubane, R. Tala-Ighil, F. Bensouici, M. Bououdina, M. Souier, S. Liu, W. Cai, A. Iratni, Sol concentration effect on ZnO nanofibers photocatalytic activity synthesized by sol–gel dip coating method, Mater. Res. Express 4 (2017) 035023.
[180] M.R. Islam, M. Rahman, S.F.U. Farhad, J. Podder, Structural, optical and photocatalysis properties of sol–gel deposited Al-doped ZnO thin films, Surface. Interfac. 16 (2019) 120–126.
[181] K. Thongsuriwong, P. Amornpitoksuk, S. Suwanboon, Photocatalytic and antibacterial activities of Ag-doped ZnO thin films prepared by a sol–gel dip-coating method, J. Sol. Gel Sci. Technol. 62 (2012) 304–312.
[182] M.N. Ghazzal, N. Chaoui, M. Genet, E.M. Gaigneaux, D. Robert, Effect of compressive stress inducing a band gap narrowing on the photoinduced activities of sol–gel TiO_2 films, Thin Solid Films 520 (2011) 1147–1154.
[183] I.A. Neacşu, A.I. Nicoară, O.R. Vasile, B.Ş. Vasile, Chapter 9 - inorganic micro- and nanostructured implants for tissue engineering, in: A.M. Grumezescu (Ed.), Nanobiomaterials in Hard Tissue Engineering, William Andrew Publishing, 2016, pp. 271–295.
[184] A. Hosseini, K.Ç. Içli, M. Özenbaş, Ç. Erçelebi, Fabrication and characterization of spin-coated TiO_2 films, Energy Proc. 60 (2014) 191–198.
[185] R.-C. Suciu, M.-C. Rosu, D. Silipas, A. Biriş, I. Bratu, E. Indrea, TiO_2 thin films prepared by spin coating technique, Rev. Roum. Chem. 56 (2011) 607–612.
[186] Y. Natsume, H. Sakata, Zinc oxide films prepared by sol-gel spin-coating, Thin Solid Films 372 (2000) 30–36.
[187] N.B. Patil, A.R. Nimbalkar, M.G. Patil, ZnO thin film prepared by a sol-gel spin coating technique for NO_2 detection, Mater. Sci. Eng. B 227 (2018) 53–60.
[188] S. Nandy, K.H. Chae, Chapter 17 - chemical synthesis of ferrite thin films, in: J. Pal Singh, K.H. Chae, R.C. Srivastava, O.F. Caltun (Eds.), Ferrite Nanostructured Magnetic Materials, Woodhead Publishing, 2023, pp. 309–334.
[189] N.-T. Nguyen, Chapter 4 - fabrication technologies, in: N.-T. Nguyen (Ed.), Micromixers, second ed., William Andrew Publishing, Oxford, 2012, pp. 113–161.
[190] A. Mishra, N. Bhatt, A.K. Bajpai, Chapter 12 - nanostructured superhydrophobic coatings for solar panel applications, in: P. Nguyen Tri, S. Rtimi, C.M. Ouellet Plamondon (Eds.), Nanomaterials-Based Coatings, Elsevier, 2019, pp. 397–424.
[191] Y. Yan, J. Li, Q. Liu, P. Zhou, Evaporation effect on thickness distribution for spin-coated films on rectangular and circular substrates, Coatings 11 (2021) 1322.
[192] B.S. Yilbas, A. Al-Sharafi, H. Ali, Chapter 3 - surfaces for self-cleaning, in: B. S. Yilbas, A. Al-Sharafi, H. Ali (Eds.), Self-Cleaning of Surfaces and Water Droplet Mobility, Elsevier, 2019, pp. 45–98.
[193] N. Sahu, B. Parija, S. Panigrahi, Fundamental understanding and modeling of spin coating process: a review, Indian J. Phys. 83 (2009) 493–502.
[194] Y. Yusuf, R.a. Syahidah Azis, M. Syazwan Mustaffa, Chapter 13 - spin-coating technique for fabricating nickel zinc nanoferrite ($Ni_{0.3}Zn_{0.7}Fe_2O_4$) thin films, in: J. A. Perez-Taborda, A.G. Avila Bernal (Eds.), Coatings and Thin-Film Technologies, IntechOpen, 2019, pp. 259–276.
[195] M.G. Buonomenna, Chapter 14 - smart composite membranes for advanced wastewater treatments, in: M.F. Montemor (Ed.), Smart Composite Coatings and Membranes, Woodhead Publishing, 2016, pp. 371–419.
[196] A. Boudrioua, M. Chakaroun, A. Fischer, Chapter 2 - organic light-emitting diodes, in: A. Boudrioua, M. Chakaroun, A. Fischer (Eds.), Organic Lasers, Elsevier, 2017, pp. 49–93.

[197] J.X.J. Zhang, K. Hoshino, Chapter 2 - fundamentals of nano/microfabrication and scale effect, in: J.X.J. Zhang, K. Hoshino (Eds.), Molecular Sensors and Nanodevices, second ed., Academic Press, 2019, pp. 43–111.
[198] W. Mekprasart, T. Khumtong, J. Rattanarak, W. Techitdheera, W. Pecharapa, Effect of nitrogen doping on optical and photocatalytic properties of TiO_2 thin film prepared by spin coating process, Energy Proc. 34 (2013) 746–750.
[199] H.-J. Lin, T.-S. Yang, C.-S. Hsi, M.-C. Wang, K.-C. Lee, Optical and photocatalytic properties of Fe^{3+}-doped TiO_2 thin films prepared by a sol–gel spin coating, Ceram. Int. 40 (2014) 10633–10640.
[200] G. Poongodi, P. Anandan, R.M. Kumar, R. Jayavel, Studies on visible light photocatalytic and antibacterial activities of nanostructured cobalt doped ZnO thin films prepared by sol–gel spin coating method, Spectrochim. Acta: Mol. Biomol. Spectrosc. 148 (2015) 237–243.
[201] M.I. Badawy, F.A. Mahmoud, A.A. Abdel-Khalek, T.A. Gad-Allah, A.A. Abdel Samad, Solar photocatalytic activity of sol–gel prepared Ag-doped ZnO thin films, Desalination Water Treat. 52 (2014) 2601–2608.
[202] D.A.H. Hanaor, G. Triani, C.C. Sorrell, Morphology and photocatalytic activity of highly oriented mixed phase titanium dioxide thin films, Surf. Coat. Technol. 205 (2011) 3658–3664.
[203] N.F.d. Andrade Neto, R.G.d. Carvalho, L.M.P. Garcia, R.M. Nascimento, C. A. Paskocimas, E. Longo, M.R.B. Delmonte, F.V.d. Motta, Influence of doping with Sm^{3+} on photocatalytic reuse of ZnO thin films obtained by spin coating, Rev. Mater. 24 (2019) 4.
[204] C.-Y. Wu, Y.-L. Lee, Y.-S. Lo, C.-J. Lin, C.-H. Wu, Thickness-dependent photocatalytic performance of nanocrystalline TiO_2 thin films prepared by sol–gel spin coating, Appl. Surf. Sci. 280 (2013) 737–744.
[205] C. Falcony, M. Aguilar-Frutis, M. García-Hipólito, Spray pyrolysis technique; High-K dielectric films and luminescent materials: a review, Micromachines 9 (2018) 414.
[206] O. Malik, F.J.D.L. Hidalga-Wade, R.R. Amador, Chapter 8 - spray pyrolysis processing for optoelectronic applications, in: M. Samer (Ed.), Pyrolysis, IntechOpen, 2017, pp. 197–219.
[207] J. Leng, Z. Wang, J. Wang, H.-H. Wu, G. Yan, X. Li, H. Guo, Y. Liu, Q. Zhang, Z. Guo, Advances in nanostructures fabricated via spray pyrolysis and their applications in energy storage and conversion, Chem. Soc. Rev. 48 (2019) 3015–3072.
[208] M. Awale, S.D. Lokhande, S.S. Jadhav, S.B. Kadam, V.D. Mote, A.B. Kadam, Effect on ethanol sensing ability of zinc oxide thin films with manganese doping, J. Mater. Sci. Mater. Electron. 34 (2023) 934.
[209] D. Perednis, L. Gauckler, Thin film deposition using spray pyrolysis, J. Electroceram. 14 (2005) 103–111.
[210] K. Pierściński, T. Piwonski, T. Ochalski, K. Emil, D. Pierścińska, M. Bugajski, Analysis of mounting induced strain in semiconductor structures by means of spatially resolved optical modulation techniques, Opt. Appl. 35 (2005) 605–610.
[211] N. Khan, J. Li, Effects of compressive strain on optical properties of $In_xGa_{1-x}N$/GaN quantum wells, Appl. Phys. Lett. 89 (2006) 151916.
[212] V. Swamy, A.Y. Kuznetsov, L.S. Dubrovinsky, A. Kurnosov, V.B. Prakapenka, Unusual compression behavior of anatase TiO_2 nanocrystals, Phys. Rev. Lett. 103 (2009) 075505.
[213] R. Kusano, T. Hiyoshi, A. Yonezu, Estimation method of residual stress and plastic strain in austenitic stainless steel by single indentation test, in: L. Ye (Ed.), Recent Advances in Structural Integrity Analysis - Proceedings of the International Congress (APCF/SIF-2014), Woodhead Publishing, Oxford, 2014, pp. 555–559.
[214] P. Waters, A.A. Volinsky, Stress and moisture effects on thin film buckling delamination, Exp. Mech. 47 (2006) 163–170.
[215] D. Li, J. Zhang, L. Shao, C. Chen, G. Liu, Y. Yang, Preparation and photocatalytic properties of nanometer TiO_2 thin films by improved ultrasonic spray pyrolysis, Rare Met. 30 (2011) 233–237.
[216] N. Narayanan, N.K. Deepak, Amelioration of photocatalytic activity of ZnO thin films by Er doping, J. Mater. Sci. Mater. Electron. 29 (2018) 8774–8784.
[217] V. Mata, A. Maldonado, M. de la Luz Olvera, Deposition of ZnO thin films by ultrasonic spray pyrolysis technique. Effect of the milling speed and time and its application in photocatalysis, Mater. Sci. Semicond. Process. 75 (2018) 288–295.
[218] N.S. Portillo-Vélez, M. Bizarro, Sprayed pyrolyzed ZnO films with nanoflake and nanorod morphologies and their photocatalytic activity, J. Nanomater. 2016 (2016) 5981562.
[219] H. Sutanto, S. Wibowo, I. Nurhasanah, E. Hidayanto, H. Hadiyanto, Ag doped ZnO thin films synthesized by spray coating technique for methylene blue photodegradation under UV irradiation, Int. J. Chem. Eng. 2016 (2016) 6195326.
[220] S. Rahemi Ardekani, A. Rouhaghdam, M. Nazari, N-doped ZnO-CuO nanocomposite prepared by one-step ultrasonic spray pyrolysis and its photocatalytic activity, Chem. Phys. Lett. 705 (2018) 19–22.
[221] H. Sutanto, I. Alkian, M. Mukholit, A.A. Nugraha, E. Hidayanto, I. Marhaendrajaya, P. Priyono, Analysis of Fe-doped ZnO thin films for degradation of rhodamine b, methylene blue, and Escherichia coli under visible light, Mater. Res. Express 8 (2021) 116402.
[222] L. Denardo, G. Raffaini, F. Ganazzoli, R. Chiesa, Chapter 5 - metal surface oxidation and surface interactions, in: R. Williams (Ed.), Surface Modification of Biomaterials, Woodhead Publishing, 2011, pp. 102–142.
[223] B.K. Chakrabarti, M. Gençten, G. Bree, A.H. Dao, D. Mandler, C.T.J. Low, Modern practices in electrophoretic deposition to manufacture energy storage electrodes, Int. J. Energy Res. 46 (2022) 13205–13250.
[224] C. Augello, H. Liu, Chapter 12 - surface modification of magnesium by functional polymer coatings for neural applications, in: T.S.N.S. Narayanan, I.-S. Park, M.-H. Lee (Eds.), Surface Modification of Magnesium and its Alloys for Biomedical Applications, Woodhead Publishing, 2015, pp. 335–353.
[225] S.M. Best, P.C. Marti, Chapter 2 - mineral coatings for orthopaedic applications, in: M. Driver (Ed.), Coatings for Biomedical Applications, Woodhead Publishing, 2012, pp. 43–74.
[226] A.R. Bhatti, P.M. Farries, 4.21 - preparation of long-fiber-reinforced dense glass and ceramic matrix composites, in: A. Kelly, C. Zweben (Eds.), Comprehensive Composite Materials, Pergamon, Oxford, 2000, pp. 645–667.
[227] S. Hu, W. Li, H. Finklea, X. Liu, A review of electrophoretic deposition of metal oxides and its application in solid oxide fuel cells, Adv. Colloid Interface Sci. 276 (2020) 102102.
[228] M. Mozafari, A. Ramedani, Y.N. Zhang, D.K. Mills, Chapter 8 - thin films for tissue engineering applications, in: H.J. Griesser (Ed.), Thin Film Coatings for Biomaterials and Biomedical Applications, Woodhead Publishing, 2016, pp. 167–195.
[229] P. Amrollahi, J.S. Krasinski, R. Vaidyanathan, L. Tayebi, D. Vashaee, Electrophoretic deposition (EPD): fundamentals and applications from nano- to micro-scale structures, in: M. Aliofkhazraei, A.S. Hamdy Makhlouf (Eds.), Handbook of Nanoelectrochemistry: Electrochemical Synthesis Methods, Properties and Characterization Techniques, Springer International Publishing, Cham, 2015, pp. 1–27.
[230] A.R. Boccaccini, S. Keim, R. Ma, Y. Li, I. Zhitomirsky, Electrophoretic deposition of biomaterials, J. R. Soc. Interface 7 (2010) S581–S613.
[231] M. Ghaemmaghami, Y. Yamini, H. Amanzadeh, B. Hosseini Monjezi, Electrophoretic deposition of ordered mesoporous carbon nitride on a stainless steel wire as a high-performance solid phase microextraction coating, Chem. Commun. (J. Chem. Soc. Sect. D) 54 (2018) 507–510.
[232] J.-C. Chou, S.-C. Lin, Y.-H. Liao, J.-E. Hu, S.-W. Chuang, C.-H. Huang, The influence of electrophoretic deposition for fabricating dye-sensitized solar cell, J. Nanomater. 2014 (2014) 126053.
[233] M.M. Mohammadi, M. Vossoughi, M. Feilizadeh, D. Rashtchian, S. Moradi, I. Alemzadeh, Effects of electrophoretic deposition parameters on the photocatalytic activity of TiO_2 films: optimization by response surface methodology, Colloids Surf. A Physicochem. Eng. Asp. 452 (2014) 1–8.
[234] C. Pablos, J. Marugán, R. van Grieken, P. Dunlop, J. Hamilton, D. Dionysiou, J. Byrne, Electrochemical enhancement of photocatalytic disinfection on aligned TiO_2 and nitrogen doped TiO_2 nanotubes, Molecules 22 (2017) 704.
[235] Z. Hosseini, N. Taghavinia, N. Sharifi, M. Chavoshi, M. Rahman, Fabrication of high conductivity TiO_2/Ag fibrous electrode by the electrophoretic deposition method, J. Phys. Chem. C 112 (2008) 18686–18689.
[236] V. Teodoro, E. Junior, M. vianna nogueira, M. Zaghete, E. Longo, L. Perazolli, Photocatalytic activity of Cu doped TiO_2 films deposited by electrophoresis, Sci. Revs. Chem. Commun. 7 (2017) 112.
[237] R. Jothi Ramalingam, Surface and electrochemical characterization of N-Fe-doped-TiO_2 nanoparticle prepared by hydrothermal and facile electro-deposition method for visible light driven pollutant removal, Int. J. Electrochem. Sci. 12 (2017) 797–811.
[238] A.K. Singh, U.T. Nakate, TiO_2 microwave synthesis, electrophoretic deposition of thin film, and photocatalytic properties for methylene blue and methyl red dyes, ISRN Nanotechnol. 2014 (2014) 326747.
[239] R. Zouzelka, M. Remzova, J. Plsek, L. Brabec, J. Rathousky, Immobilized rGO/TiO_2 photocatalyst for decontamination of water, Catalysts 9 (2019) 708.
[240] S.E. Hosseini Yeganeh, M. Kazazi, B. Koozegar Kaleji, S.H. Kazemi, B. Hosseinzadeh, Electrophoretic deposition of Sn-doped TiO_2 nanoparticles and its optical and photocatalytic properties, J. Mater. Sci. Mater. Electron. 29 (2018) 10841–10852.
[241] H. Azizi-Toupkanloo, M. Karimi-Nazarabad, G.-R. Amini, A. Darroudi, Immobilization of AgCl@TiO_2 on the woven wire mesh: sunlight-responsive environmental photocatalyst with high durability, Sol. Energy 196 (2020) 653–662.
[242] A. Ben Youssef, N. Barbana, M. Al-Addous, L. Bousselmi, Preparation and characterization of photocatalytic TiO_2/WO_3 films on functionalized stainless steel, J. Mater. Sci. Mater. Electron. 29 (2018) 19909–19922.
[243] M. Zlamal, J.M. Macak, P. Schmuki, J. Krýsa, Electrochemically assisted photocatalysis on self-organized TiO_2 nanotubes, Electrochem. Commun. 9 (2007) 2822–2826.
[244] J.M. Macak, M. Zlamal, J. Krysa, P. Schmuki, Self-organized TiO_2 nanotube layers as highly efficient photocatalysts, Small 3 (2007) 300–304.
[245] E. Mohammadi, M. Aliofkhazraei, A.S. Rouhaghdam, In-situ study of electrophoretic deposition of zinc oxide nanosheets and nanorods, Ceram. Int. 44 (2018) 1471–1482.
[246] Y.-C. Wang, I.-C. Leu, M.-H. Hon, Kinetics of electrophoretic deposition for nanocrystalline zinc oxide coatings, J. Am. Ceram. Soc. 87 (2004) 84–88.
[247] B.-S. Jun, Preparation of ZnO thin film by electrophoretic deposition (EPD), J. Korean Ceram. Soc. 49 (2012) 78.
[248] M. Taheri, H. Abdizadeh, M.R. Golobostanfard, Formation of urchin-like ZnO nanostructures by sol-gel electrophoretic deposition for photocatalytic application, J. Alloys Compd. 725 (2017) 291–301.
[249] A.H. Navidpour, J. Safaei, G. Zhang, A. Mojiri, B.-J. Ni, Z. Huang, J. Zhou, Photocatalytic and photoelectrocatalytic degradation of perfluorooctanoic acid by immobilised ZnO nanoparticles using electrophoretic deposition, Environ. Sci.: Nano 10 (2023) 1955–1965.